THE STRENGTHENING EFFECT OF ORDERED PRECIPITATES IN A Ni-Ni_4Mo SYSTEM

A THESIS

Presented to

The Faculty of the Division of Graduate

Studies and Research

By

John Wesley Goodrum

In Partial Fulfillment

of the Requirements for the Degree

Doctor of Philosophy in the School

of Chemical Engineering

Georgia Institute of Technology

August, 1974

THE STRENGTHENING EFFECT OF ORDERED PRECIPITATES

IN A Ni-Ni_4Mo SYSTEM

Approved:

Bruce G. LeFevre, Chairman

Edgar A. Starke, Jr.

Robert F. Hochman

Date approved by Chairman: 7-19-74

ACKNOWLEDGMENTS

The author is greatly indebted to Dr. Bruce G. LeFevre for guidance in graduate work in general and in the preparation of this thesis. The advice and suggestions of Dr. E. A. Starke, Jr., are gratefully acknowledged. Also, the author would like to thank the other members of the Metallurgy staff and fellow graduate students for help and suggestions given many times during this study.

The author wishes to thank his wife Rosemarie for her encouragement and patience during the course of this work.

TABLE OF CONTENTS

TABLE OF CONTENTS (Continued)

LIST OF TABLES

LIST OF ILLUSTRATIONS

LIST OF ILLUSTRATIONS (Continued)

SUMMARY

Ni-Ni_4Mo alloys of two compositions (14 at.% and 17 at.% Mo) were studied by transmission electron microscopy and mechanical testing. Yield stress, hardness, particle size, particle orientation, lattice order and dislocation configurations were measured after isothermal aging at 700°C, 750°C, and 800°C. Temperature dependence of yield stress was measured after isothermal aging at 750°C.

The 17 at.% solid solution decomposed to a uniform dispersion of ordered, cuboidal Ni_4Mo particles and disordered solid solution at 750°C. The $(001)_{tet}$ face of the precipitate is parallel to $(001)_{fcc}$ of the matrix. Particle growth rate is proportional to $(\text{time})^{1/3}$. The yield stress as a function of particle size shows a close correlation to the calculated flow stress due to shear of ordered particles by five-unit superdislocations. The yield stress is also suggested to be partially dependent on matrix/precipitate lattice misfit since flow stress shows an inverse temperature dependence.

CHAPTER I

INTRODUCTION

During precipitation in two phase Ni-Ni_4Mo systems, large hardness and strength changes are observed. Both the effects of normal precipitation hardening and order hardening, due to order in the precipitate lattice, may be seen. These are controlled to a large extent by the nature of the decomposition process which includes the possibilities of heterogeneous and homogeneous nucleation and growth and evolution of modulated structure [1,2].

Ni-Mo alloys are worthy of study because, aside from their intrinsic interest as unresearched alloys, they can provide a test of deformation theories. These alloys, which form ordered precipitates in a disordered matrix, can be used to test the generality of deformation theories that, for example, explain the behavior of Ni-Ni_3Al [3,4]. From the standpoint of commercial application, Ni with the addition of Mo has most of the basic properties associated with super-alloys. A Ni base, age hardening properties, and probable coherent precipitate [5,6,7] are found in the 12 to 20 at.% Mo alloys (See Figure 1). Since commercial superalloys may contain up to eight elements, the binary Ni-Mo system makes the isolation of variables for study easier.

In the superalloys, optimum strengthening occurs if the precipitate phase is a fine, (e.g. 100A) uniform dispersion, coherent

with the matrix. From the known lattice parameter of Ni_4Mo and Ni-Mo alloys, [7], it was expected that Ni-Ni_4Mo alloys would have coherent precipitates. However, precipitate size and dispersion vary with alloy composition and temperature at which the precipitate phase separates from the solid solution. A preliminary survey of several Ni-Ni_4Mo compositions and aging temperatures was conducted in this study in order to find a suitable precipitate microstructure. The alloy selected for study has a relatively high volume fraction of ordered Ni_4Mo precipitates. For many alloys with a large volume fraction of coherent precipitates, dislocations shear the precipitates during deformation [8]. The shearing process may be controlled by either order within the precipitates or strain fields due to precipitate/matrix lattice misfit.

Assuming that precipitate shear is experimentally proven, evidence of either strain field or order strengthening is required for an explanation of the strengthening mechanism. For a given microstructure, a coherency strain mechanism and an order mechanism predict different values for the flow stress, or alloy strength. Also, the temperature dependence of flow stress is different for these mechanisms. The particle size function of flow stress, and other secondary experimental evidence should further indicate which mechanism is operating in the alloy.

The general objectives in this research were (i) to determine which Ni-Ni_4Mo composition and heat treatment would yield a fine particle dispersion suitable for precipitate strengthening studies, and (ii) to sort out the strengthening mechanisms by suitable

experimental measurements. As is shown later, this reduced to a choice between the relative roles of coherency strain hardening and order hardening. The approach used was to select a two-phase alloy with about 0.3 volume fraction of cubic precipitates. Aged alloys were pulled in tension over a range of temperature and examined by TEM to determine microstructures and basic deformation characteristics such as deformation by slip, particle shearing, and dislocation pairs, etc. In the following chapters of this thesis, models of deformation and experimental details of the alloy aging process are presented. Experimental results are compared with theoretical predictions of various deformation models.

CHAPTER II

DEFORMATION MODELS RELEVANT TO Ni-Ni_4Mo ALLOYS

2.1 General Description of Models

The primary purpose of this work is to characterize deformation mechanisms of a precipitation strengthened Ni-Ni_4Mo alloy. This will be attempted from microstructural characterization and analysis of the mechanical properties in terms of proposed deformation models. There are two general models for precipitate-hardened alloys which explain deformation in terms of dislocation/precipitate interactions, one dealing with precipitate shearing and the other with precipitate looping (Orowan mechanism) [41].

For many nickel-base alloys with large volume fraction of coherent ordered precipitates, precipitate shearing involving either order strengthening or coherency strain has been sufficient to account for the experimental flow stress and dislocation microstructure [28]. For Ni-Ni_4Mo alloys which have these general properties, the flow stress should fit one of the above shearing models. In the last section of this chapter we will present additional arguments in favor of a shearing rather than looping mode of deformation in many of the Ni-Ni_4Mo alloys. The shearing models assume that there is a uniform dispersion of relatively small precipitates. Order strengthened systems contain ordered particles which shear to form a high energy lattice state (APB) within the precipitate

during deformation. "Coherency strain" models assume a precipitate/matrix lattice misfit which generates a strain field around the precipitate and thereby opposes the movement of dislocations.

In order to choose between possible mechanisms of deformation in an alloy, the mechanical strength as a function of precipitate microstructure must first be known. Also various microstructural parameters such as particle size, lattice misfit of precipitates, and lattice order, are needed for a calculation of flow stress. Thus a careful study of specific alloy characteristics is necessary before the appropriate deformation mechanism can be selected.

To deal with the complex interactions of one or more dislocations which cut through precipitate particles, simplifying assumptions must be made. Only a/2 [110] (111) dislocations will be considered in this work. The assumption that all deformation is due to such dislocations is often made in models of strengthening by ordered coherent precipitates in fcc materials [15], and many systems which have ordered coherent precipitates are known to deform by a/2 [110] (111) dislocations [8,18]. Further, Shockly partials were not observed in deformed 20 at.% Ni-Mo [14].

2.2 Deformation Related Properties of Ni-Ni_4Mo

2.2.1 Alloy Microstructures

Previous work with the Ni-Mo system [9,10] has established that there is a two-phase region extending from about 12 at.% to 20 at.% Mo in which the nickel rich solid solution (α) and the ordered phase Ni_4Mo (β) are in equilibrium at room temperature (See

Figure 1). By quenching from above the solvus line, a single phase (α) structure is retained at room temperature. Subsequent aging below the solvus line results in age hardening across the 12 to 20 at.% region [9,10]. Stoichiometric Ni_4Mo orders from fcc to a tetragonal lattice when the quenched alloy is aged [5,6,10]. Ni_4Mo (DI_8 type structure, 11) was studied by researchers [12,13] who found that the ordering processes are observable on an atomic scale by FIM. Ruedl, et al. and Saburi have related the occurrence of order to distinct electron diffraction superlattice patterns [5,13]. Brooks and Spruiell [14] using TEM observed the microstructure of aged Ni_4Mo before and after deformation.

At compositions away from the 20 at.% alloy, much less is known about the properties of the alloys. Ellenger [9] showed with hardness curves that the alloys age slowly (maximum hardness after 200 to 500 hours at 700°C) and form a beta phase visible with optical metallography. Aging gives a beta precipitate with a very similar Widmanstatten structure when any alloy in the 12 to 20 at.% Mo range is aged about 200 hours [9,10]. The known superlattice lines of Ni_4Mo are also seen in the Debye x-ray diffraction patterns of aged alloys in the 12 to 20 at.% range [10]. It is therefore reasonable to expect that (i) quenched alloys in the 12 to 20 at.% region will age by precipitating ordered Ni_4Mo particles in a disordered matrix. Further, (ii) since the precipitate lattice misfit is approximately one percent, and since Ni_4Mo is a distorted cubic lattice [22], one may expect the precipitates to have a cubic morphology [8,21,38].

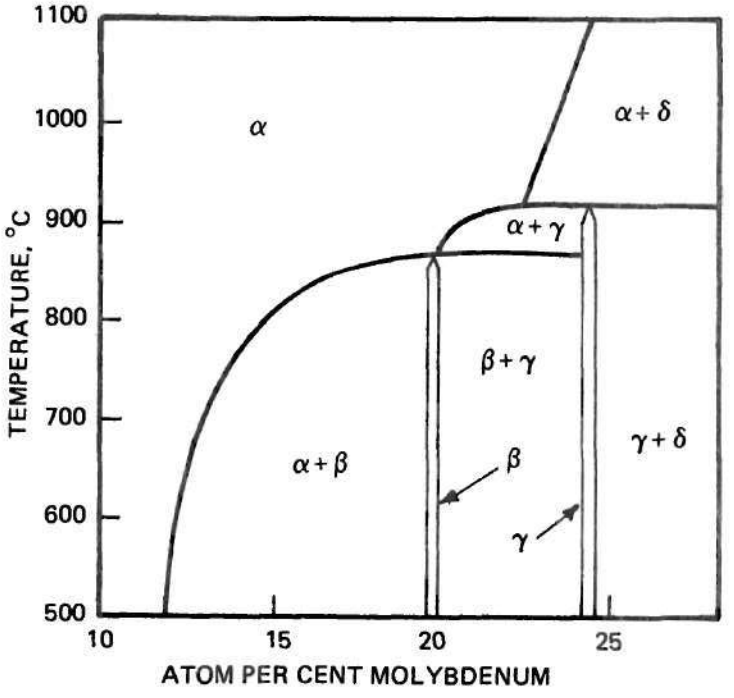

Figure 1. The Nickel-Rich Portion of the Ni-Mo System. (After Guthrie and Stansbury, 7)

2.2.2 Crystallography Relevant to Deformation Models

As pointed out in the beginning of this chapter, it is necessary to know several crystallographic variables before either of the shearing models can be compared to a specific alloy. These variables are lattice/precipitate misfit, atomic stacking in the slip plane of ordered precipitates, the interaction of dislocations with specific variants, and the probable slip planes for the precipitate and the matrix. fcc Miller indices will be used for lattice directions and planes in both phases, so that the difficulty in comparing fcc (matrix) and fct (Ni_4Mo) indices will be avoided.

Quenched Ni-Mo alloys are fcc solid solutions [7]. As discussed in the previous section, a two-phase structure of ordered Ni_4Mo and disordered fcc matrix is expected when 12 to 20 at.% compositions are aged below the solvus line. There is lattice misfit between the matrix and the ordered Ni_4Mo precipitates which can be calculated from lattice parameter data. The misfit parameter ϵ is defined as $\epsilon = (a_p - a_m)/a_m$, where a_p and a_m are respectively the precipitate and matrix lattice parameters [3]. For example, if equilibrium is attained between the matrix and precipitate phases in 17 at.% Mo at 750°C, the equilibrium tie line corresponds to a mixture of Ni_4Mo and 14 at.% solid solution. Guthrie and Stansbury [7] have measured the lattice unit cell parameters for these compositions. Using their values, one may calculate the lattice misfit of Ni_4Mo precipitates for a given Ni-Mo composition. For various compositions across the 12 to 20 at.% range, Ni_4Mo has a calculated misfit contraction of 0 to 1.2 percent along the fcc [001], and 1.2 percent to

0.5 percent misfit expansion along the fcc [100] and [010]. In earlier studies [11], coherency strains appear to account for the age strengthening in 20 at.% Mo alloy which has a large misfit (1.2 percent) in only one of three othogonal lattice directions. The comparable particle misfit in alloys across the 12 to 20 at.% region suggests that coherency strain could account for any age-induced strengthening observed at these compositions.

2.2.3 Variant Interaction with Dislocations

The influence of specific variants on slip processes must be evaluated. (It is assumed that each particle is a single order variant; "variant" and "particle" are used interchangeably in this study.) One must consider whether all the variants uniformly impede slip in a given slip system. Six crystallographically distinct order variants of Ni_4Mo may nucleate on the fcc solid solution lattice (See Figure 2). On each {100} fcc, two variants are possible, i.e., two ordered lattices may nucleate with a rotation of $\pm$ 18° from the <100> of the fcc lattice. As discussed in section 2.2.1, it is expected that the precipitates will be coherent and have a cubic morphology. Due to lattice coherency between particles and matrix, the glide planes of the precipitates are parallel to the matrix glide planes. The slip system is to some extent perturbed by the presence of strain fields around precipitates or by the need to supply APB energy within precipitates, but easy glide should remain on {111}. In Figure 3 can be seen the atomic arrangement on the close packed plane of ordered Ni_4Mo. This schematic assumes that the close packed plane of Ni_4Mo is equivalent to a close packed fcc {111} in

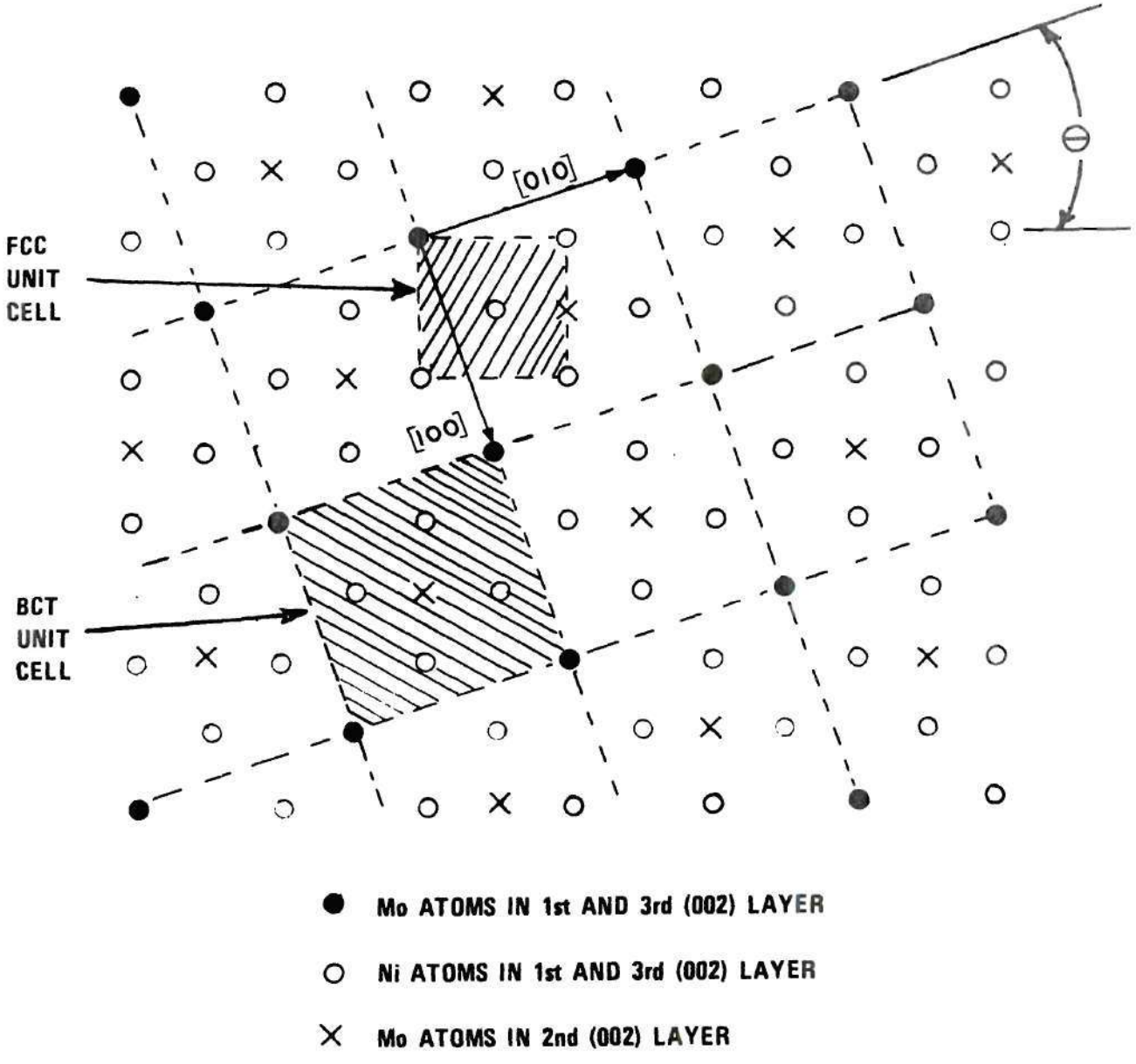

Figure 2. Schematic View of the Crystal Structure of Ni_4Mo, Viewing the Atomic Packing in (002) Planes. The 1st and 3rd Layers Coincide Exactly. Ni Atoms in the 2nd Layer are Not Shown. (After LeFevre, 12)

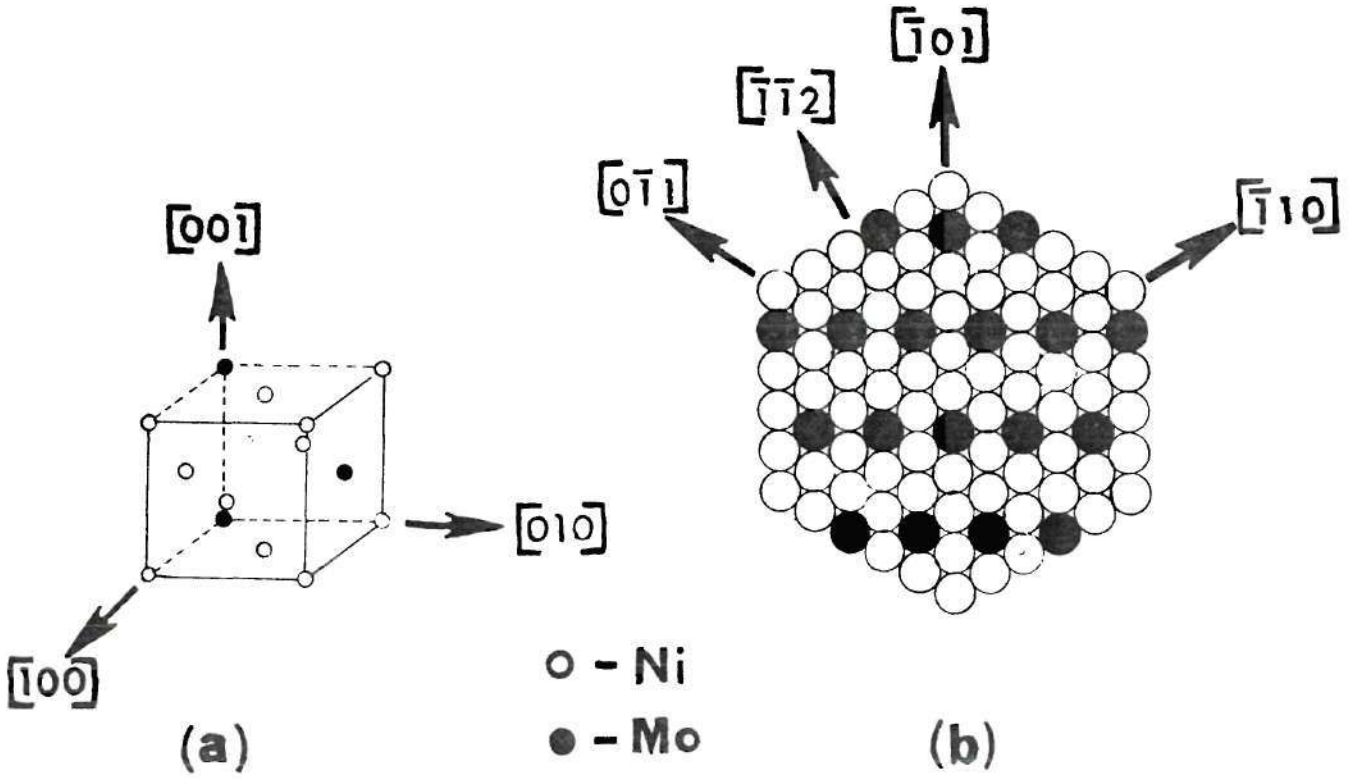

Figure 3. Atomic Stacking in the Slip Plane of Ordered Ni_4Mo. (a) Ordered Atomic Positions Relative to a fcc Lattice. (b) Close-packed Plane of Ni_4Mo. Matrix (fcc) Directions Shown.

which the atoms have ordered positions, since the ordering of fcc Ni-Mo solid solution leads to lattice shifts of one percent or less for most of the Ni-Ni_4Mo alloys. Notice that the stacking along all the <110> has the same sequence of atoms. This means that order strengthening effects should have the same magnitude along all <110>. Assuming spherical particles, the passage of a given set of <110> dislocations on a given {111} will cause the same net APB change in each order variant, and therefore all variants may be considered crystallographically equivalent with respect to order hardening.

From these observations one can see that Ni-Ni_4Mo systems may be strengthened by APB formation in ordered Ni_4Mo precipitates. Lattice misfit between matrix and precipitate generates coherency strain fields around the precipitates. These fields may impede dislocation movement and thereby strengthen a Ni-Ni_4Mo alloy. In the following sections, the equations for the shear stresses predicted by ordered-particle and strain field models are discussed.

2.3 Strengthening Due to Shear of Ordered Precipitates

2.3.1 General

Dislocation models of order strengthening in precipitate-hardened alloys will be discussed in this section. Essentially, the energy required to shear ordered precipitates will be quantitatively related to the energy needed to deform a specimen of polycrystalline alloy. All the order-hardening models discussed in this study assume that only order hardening is present and that the alloy has a uniform dispersion of identical spherical particles which randomly intersect

the slip plane. For any system hardened by ordering, the predicted shear stress required to move an edge dislocation is twice the stress needed to move a screw dislocation [15]. Therefore, in this study, and others [15,18], it was assumed that flow stress was controlled by edge dislocations.

The basic elements of the order models are antiphase boundary, APB, energy and glide dislocation configurations (e.g. superdislocations). APB energy is directly related to the stress required to move a dislocation through an ordered lattice. A single dislocation moving through an ordered lattice, such as Figure 3, shifts the relative positions of atoms along the slip path. This is a higher energy configuration, and work (APB energy) must be added to the lattice. The above process creates a disordered lattice layer, or APB, within an ordered particle. Dislocation may occur as superdislocations in alloys with ordered precipitates [3,16]. The dislocations, of like sign, move in groups (often pairs) separated by a zone of APB (See Figure 4). This dislocation grouping has a lower energy than a single dislocation because the additional dislocations restore the lattice order by slipping adjacent lattice planes until the ordered structure is restored in the APB zone.

The results of several researches are relevant to a discussion of shear in ordered Ni_4Mo particles. Castagné [17] derived an expression for flow stress when single dislocations shear ordered precipitates. Ham [4] has mathematically treated the case of shearing by dislocation pairs. Oblak [18] has adapted the idealized models of Castagné [17], Gerald [19] and others in order to describe shear of

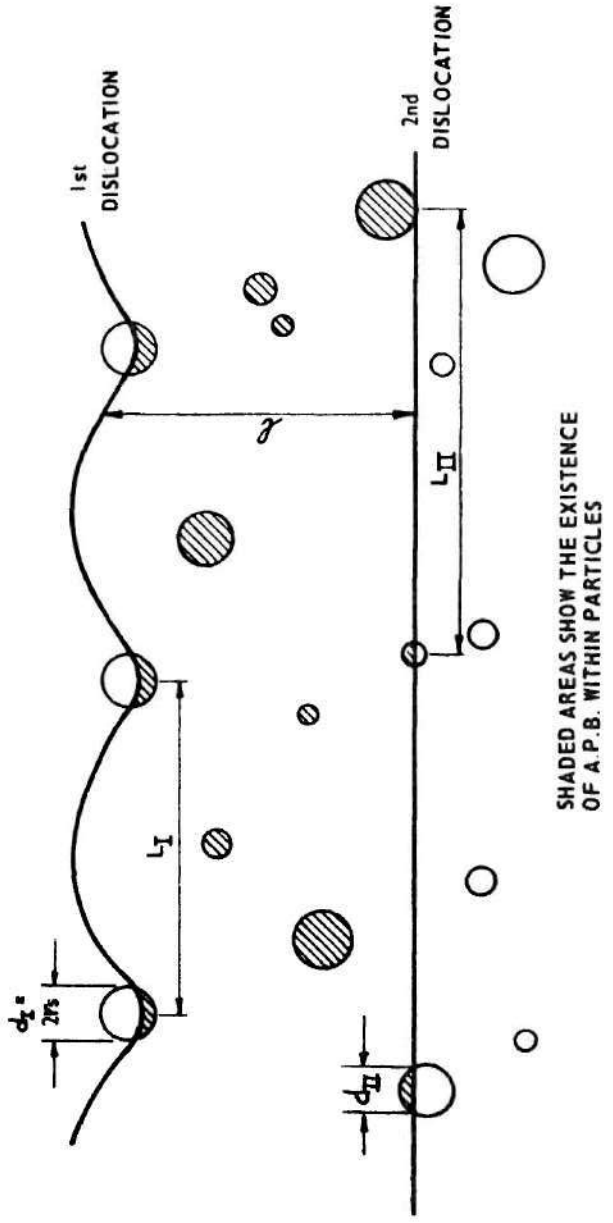

Figure 4. The Geometry of a Dislocation Pair Interacting with Ordered Precipitates. (After Ham, 4)

plate-like precipitates by 4-unit super-dislocations.

As an example of an analysis of order-induced flow stress in a specific material, R. K. Ham's study of the shear of ordered, coherent Ni_3Al particles by paired dislocations is outlined below. Ham [4,15] has a simple treatment of order strengthening which permits convenient calculation of a predicted flow stress for a given alloy. APB energy (γ) is found from analysis of experimental flow stress data. The model assumes that only order strengthening is present and that the system has a small constant volume fraction (f) of precipitate. The precipitates are taken to be spherical, and to have no lattice mismatch or elastic constant differences with the matrix. In the systems discussed by Ham, pairs of dislocations are energetically favored because the ordered Ni_3Al structure needs only one additional dislocation to restore order when sheared by a dislocation (See Figure 5). In the region where fine dispersion of precipitates forces particle shearing by dislocations, the flow stress is:

$$\Delta\tau = \left(\frac{\gamma}{2b}\right)\left[\left(\frac{4\gamma f r_s}{\pi T}\right)^{\frac{1}{2}} - f\right] \qquad (1)$$

where γ is the APB energy, T is the average line tension of the shearing dislocation, r_s is the precipitate radius, and b is the Burgers Vector.

Equation (1) predicts a linear region in the curve of flow stress versus square root of particle radius. If the linear region is exptrapolated to zero flow stress, $r_s = \frac{\pi T f}{4\gamma}$, from which one may

calculate γ. The slope of the linear region is a function of γ,b,f and T, so that again γ may be calculated.

It is helpful if some estimate of APB energy is available to compare with experimentally-derived values. Also, a theoretical estimate of APB energy may be used to calculate a flow stress, for example, in equation one. Kear [20] and others [10] have derived values for APB energy in various systems based on chemical bond energies.

For Ni-Ni_3Al [1,4], Ham found precipitate radius as a function of flow stress by extrapolating the particle size data [1] where necessary. He assumed that the volume fraction (f) of precipitate is constant during particle growth and that it is equal to the equilibrium atomic fraction as given by the Ni-Al phase diagram. The experimentally measured cube diameter of Ni_3Al precipitates is taken to be the diameter of a spherical precipitate, on the assumption that particles with an approximately cubic morphology can be treated as spherical particles [15]. In the range where precipitate shearing is predicted, there was good agreement between the experimental and theoretical flow stress curves. The curve slope corresponds to an APB energy of 134 mJ/m^2 and the intercept yields a value of 175 mJ/m^2. The APB energy estimated from bond energies is [20] 164 mJ/m^2, in good agreement with the experimental values.

2.3.2 Ni-Ni_4Mo: Modes of Order Strengthening

After the above general comments on APB mechanisms in ordered precipitates, we now turn to the Ni-Ni_4Mo alloys and consider specific mechanisms of APB-induced strengthening. Essentially the problem is

to choose between several possible dislocation geometries. The Ni-Mo alloys may be deformed by single shearing dislocations or by two or more dislocations in a superdislocation unit. In all dislocation geometries we will assume that order variants of Ni_4Mo are not distinguishable from a strengthening point of view (see Section 2.2.3). Further it will be assumed that the matrix-precipitate interfacial energy and stress due to modulus differences are a negligible fraction of the age-induced flow stress [15].

Examination of the slip plane in an ordered lattice shows the number of unit dislocations required to restore order after a single dislocation shears through the lattice on the slip plane. Figure 3 is a schematic of the close packed plane of Ni_4Mo with the nickel and molybdenum atoms in ordered positions. It can be seen that a single dislocation moving in any one of the three <110> matrix directions on that plane will result in formation of APB. Four more unit dislocations must move across in a given <110> matrix direction before the APB is eliminated in the ordered precipitate. If the Ni_4Mo precipitates are completely ordered, one might expect to see superdislocations made up of five dislocations on any one of the {111} matrix planes during slip in the Ni-Ni_4Mo alloy. As will be discussed later, there are experimental indications that groups of dislocations ($b = \frac{1}{2}[110]$) shear the ordered particles in the two-phase alloy studied.

(a) Shear by a single dislocation.

Castagne [17] has derived an expression for the flow stress required for shearing of an ordered lattice by a single dislocation:

$$\Delta\tau = (\gamma/b)(4\gamma f r_s/\pi T)^{\frac{1}{2}} \qquad (2)$$

where the variables are those named in equation (1). In Chapter V, calculated values of flow stress are used to show that ($\Delta\tau$) for a single dislocation will be much higher than the experimental flow stress of a 17 at.% Ni-Mo alloy.

(b) Shear by two-, three-, or four-unit superdislocations.

If the close packed planes of Ni_4Mo had the same atomic stacking sequence as ordered Ni_3Al (Figure 5), dislocation pairing would be expected during deformation. However, a dislocation shearing along a <110> (See Figure 3) creates APB, but the second, third or fourth dislocations do not restore any atoms to ordered positions in the lattice. Assuming only nearest neighbor interactions are important factors in the APB energy, a suitable model of the flow stress may be derived by writing a force balance equation for each unit of the superdislocation. These equations are summed to obtain the net flow stress for a given type superdislocation (See Appendix F):

for pairs of dislocations,

$$\Delta\tau = \frac{\gamma}{2b}\left(\frac{2r_1}{L_1}\right) \qquad (2a)$$

for superdislocations made up of three dislocations,

$$\Delta\tau = \frac{\gamma}{3b}\left(\frac{2r_1}{L_1}\right) \qquad (2b)$$

for four-unit superdislocations,

$$\Delta\tau = \frac{\gamma}{4b}\left(\frac{2r_1}{L_1}\right) \tag{2c}$$

In 2a, 2b, and 2c; γ is the APB energy, L_i is the effective interparticle spacing along the dislocation, and $2r_i$ is the average length of APB per particle in contact with a dislocation.

If the first dislocation has a Friedel spacing [15], then

$$\frac{2r_i}{L_i} = \left(\frac{4\gamma r_s f}{\pi T}\right)^{\frac{1}{2}}$$

where r_s is the average radius of spherical particles and T is the average line tension of the dislocation. A Friedel spacing is appropriate for a dislocation which bends slightly between the particles during shear, i.e., the Friedel spacing is appropriate for relatively weak particles. Substituting the Friedel spacing into equations 2a, 2b, and 2c yields the following expressions:

for two dislocations,

$$\Delta\tau = \frac{\gamma}{2b}\left(\frac{4\gamma f r_s}{\pi T}\right)^{\frac{1}{2}} \tag{2d}$$

for three dislocations,

$$\Delta\tau = \frac{\gamma}{3b}\left(\frac{4\gamma f r_s}{\pi T}\right)^{\frac{1}{2}} \tag{2e}$$

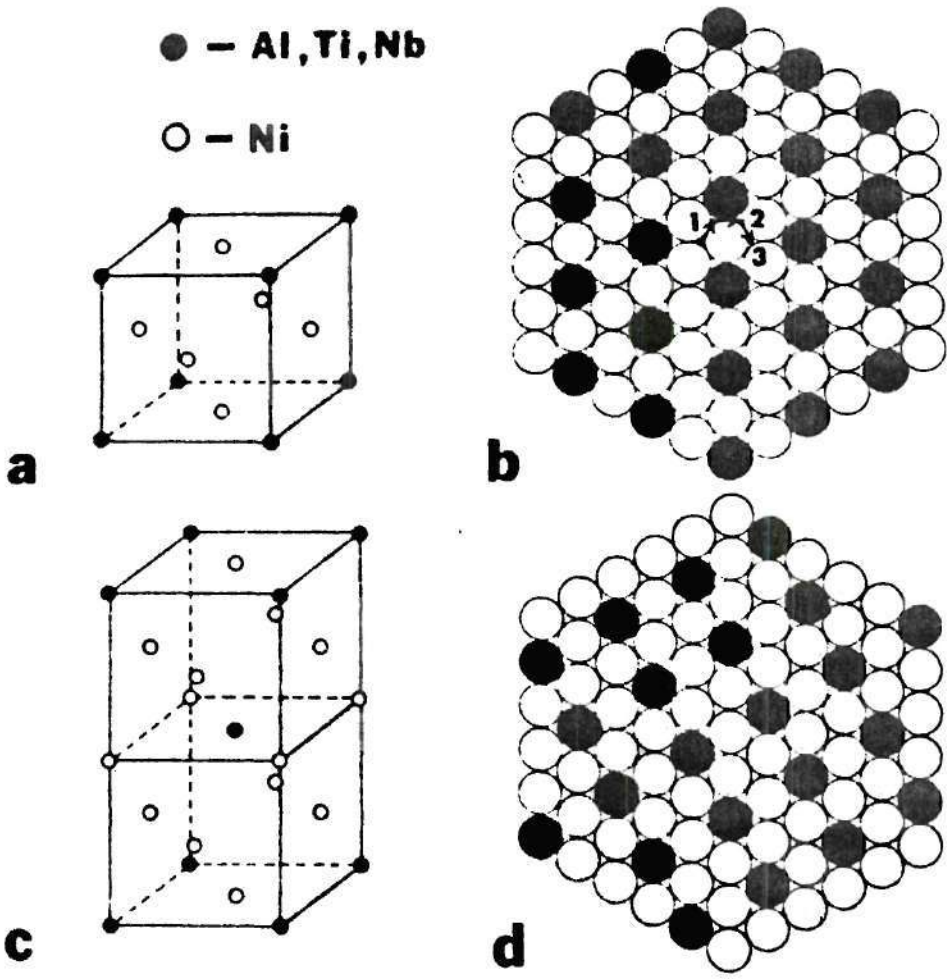

Figure 5. Two A_3B Ordered Variants of fcc. (a) Ll_2 Unit Cell. (b) Arrangement of Atoms on Ll_2 Close-packed Plane: Ordered Ni_3Al Structure. (c) DO_{22} Unit Cell. (d) Arrangement of Atoms on a DO_{22} Close-packed Plane: Ordered Ni_3Nb Structure. (After Kear, 28)

for four dislocations,

$$\Delta\tau = \frac{\gamma}{4b}\left(\frac{4\gamma f r_s}{\pi T}\right)^{\frac{1}{2}} \qquad (2f)$$

From equations 2d, 2e, and 2f; theoretical flow stresses for Ni-Ni_4Mo alloys were calculated (See Appendix D and Figure 16).

(c) Shear by five-unit superdislocations.

As mentioned earlier in this chapter, the stacking in the close packed plane of ordered Ni_4Mo particles should stabilize a five-unit superdislocation (See 2.2.2 and Figure 3). If the appropriate equations for a set of five dislocations are summed as described in the previous section, an expression for the net flow stress due to a five-unit superdislocation is obtained (See Appendix F):

$$\Delta\tau_5 = \frac{\gamma}{5b}\left[\frac{2r_1}{L_1} - \frac{2r_5}{L_5}\right] \qquad (3)$$

where the variables are those named in equation 2c.

As in equations 2a, 2b, and 2c, a Friedel spacing may be used for $2r_i/L_i$. If the fifth dislocation is straight, then $2r_5/L_5$ may be taken as f, the volume fraction [15]. The fifth dislocation restores order when it shears the Ni_4Mo lattice. Since there is negligible precipitate-induced repulsive force along the fifth dislocation line, it is reasonable to assume that the fifth dislocation will have a low energy straight configuration. Substituting these terms into equation (3) gives:

$$\Delta\tau = \frac{\gamma}{5b}\left[\left(\frac{4\gamma f r_s}{\pi T}\right)^{\frac{1}{2}} - f\right] \qquad (4)$$

An estimate of the Ni_4Mo APB energy and the line tension is needed in order to calculate a flow stress using equation [4]. γ for Ni_4Mo may be estimated from the Bragg-Williams model as applied to Ni_4Mo [10] (See Appendix C). and T may be approximated by $\frac{Gb^2}{2}$ [15].

The models of order hardening predict levels of flow stress which are functions of superdislocation geometry. If order were the only hardening factor in a Ni-Ni_4Mo alloy, it would be possible to decide which superdislocation geometry is operating in the alloy by comparing the theoretical and experimental levels of flow stress.

2.4 Coherency Strain Strengthening Model

2.4.1 General

In view of the proven lattice misfit of tetragonal Ni_4Mo precipitates in fcc Ni-Mo solid solutions in the 12 to 20 at.% Mo region, it is reasonable to examine the fit of coherency strain models to experimental Ni-Ni_4Mo flow stress data. For most compositions across the Ni-Ni_4Mo region, Ni_4Mo has a calculated misfit ϵ of about one percent in one or more orthogonal lattice directions (See section 2.2.2). Orowan and Brooks [23] predicted that for precipitates with one percent misfit (spherical), the limits of precipitate/matrix coherency are reached at particle diameters of 500A to 1000A. If the Ni_4Mo particles are near 500A in diameter, it can be assumed that large coherency strains exist at the matrix/precipitate interface in a Ni-Ni_4Mo system. However, for a given composition the

magnitude of the misfit parameter is less than one percent in one or two of the three othogonal directions, which means that the total lattice strain due to a Ni_4Mo precipitate is less than for a spherically-misfitting particle with a one percent misfit.

If an alloy contains coherent spherical precipitates which have a spherical misfit ϵ with the matrix, then the flow stress in the alloy due to lattice strains may be found from the expression (Gerald and Haberkorn, [19]):

$$\Delta\tau = 3G(\epsilon)^{3/2}\left(\frac{rf}{b}\right)^{\frac{1}{2}} \qquad (5)$$

where G is the shear modulus, r is the radius of the spherical precipitate, and ϵ is the misfit parameter (See section 2.2.2). Although there remains some controversy concerning the theoretical models of coherency strengthening, the Gerald and Haberkorn model appeared to be the most widely accepted model at the time of this study and was adopted for calculations in this work (See Appendix E for further discussion of strain models).

The properties of the precipitates in Ni-Ni_4Mo systems differ from those required for equation (5). Most of the differences, however, are small and equation (5) may be applied to the alloys if several approximations are made. First, as in the order strengthening models, it was assumed that cubic precipitates may be treated as spheres. This geometrical approximation should also be valid for coherency strain calculations. Next, the differing misfit parameters of Ni_4Mo must be combined to yield a spherical misfit parameter.

One may take the largest of the misfit values as the spherical misfit. This should be the upper limit of coherency strain strengthening in that alloy. The average of the orthogonal misfit values may be used as a spherical misfit parameter. One could average the absolute value of misfit parameters, otherwise one must deal with both compressive and tensile strain fields around the precipitates. For the case where the absolute values are nearly equal, the lattice misfit parameters are, in effect, nearly equivalent to a spherical misfit. Therefore an average of the three misfit values should be a good approximation for use as a spherical misfit parameter in equation (5). The predicted flow stress for a series of misfit values is given in Chapter V and Appendix E.

2.4.2 Temperature Dependence of Flow Stress

Since the shear modulus of most materials varies inversely with temperature, one can predict the relative temperature dependence of order and strain field strengthening models. For a strain induced flow stress which is described by equation 5, the flow stress is proportional to the shear modulus, G. Since G is inversely proportional to temperature, flow stress due to strain fields decreases with increasing temperature. On the other hand, if an APB-induced flow stress is accurately described by equation 2 or equation 5, the following relationships will hold: Flow stress due to APB energy is inversely proportional to line tension and G; therefore, flow stress should increase with increasing temperature. Oblak, et al. [18] have discussed these relationships as they apply to Ni_3Nb precipitates. In the case of a Ni-Ni_4Mo alloy, the

temperature dependence of flow stress should indicate if there is a significant coherency strain strengthening component showing a decrease in flow stress with temperature.

2.5 Orowan Model

Dislocations may bend between (Orowan looping), rather than shear through, precipitates during deformation of a precipitate-strengthened alloy. However, as discussed in section (2.1), Ni-Ni_4Mo alloys with a large volume fraction of precipitate would not be expected to deform by Orowan looping processes, primarily due to the close spacing of particles in the alloy microstructure. Several quantitative examples of the stress level required for looping in Ni-Ni_4Mo alloys are discussed below.

If the Orowan stress for an alloy about midway of the Ni-Ni_4Mo region, 17 at.%, is calculated using an expression by Hirsch and Humphries [24] for a particle diameter of 300A, then the minimum stress level for dislocation looping is 134 Kg/mm^2. In this calculation it is assumed that the precipitates are identical spheres and have a random lattice spacing on the slip plane. The flow stress equation considers the effects of dislocation loop configuration (the loop is elliptical) and the effects of the interaction of bowed segments of dislocation on the dislocation line tension (See Appendix B). The flow stress of 134 Kg/mm^2 is much higher than the flow stress predicted for 300 A Ni_4Mo particles by the five-dislocation order model for particle shearing (See Figure 16). It is reasonable to assume that Orowan looping will not occur in the above

microstructure, since one expects a system to deform by the mechanism which requires the lowest energy.

At larger particle sizes (f remaining constant) the critical stress for Orowan bypassing of particles is still a very large value. Using the above assumptions about the Ni-Ni_4Mo system, a 17 at.% alloy containing 500A particles would have a minimum flow stress of 90 Kg/mm^2. The Orowan critical stress at this particle size is three times larger than the stress required if the particles were sheared by five-unit superdislocations (See Figure 16). A particle size of 500A is near the limits of particle/matrix coherency for 17 at.% alloy (See 2.4.1) (coherency of precipitates is assumed for all microstructures in this study) and represents the microstructure most favorable to Orowan processes. Such calculations show that Orowan looping is not probable near the middle of the Ni-Ni_4Mo composition range.

For compositions to the left of 17 at.% Mo, the volume fraction is smaller and Orowan looping probably could occur at some point, if the precipitate size were 300A to 500A. For compositions greater than 17 at.% Mo, dislocation looping around precipitates is less probable, due to the larger fraction of precipitate phase. Again, it is assumed that the precipitates will be about 500A in diameter.

CHAPTER III

EXPERIMENTAL METHODS

3.1 Alloy Preparation and Preliminary Experiments

The alloys for this study were prepared in 75g bars by arc melting Ni (99.97 percent) and Mo (99.99 percent) in an argon atmosphere. Mixing was improved by turning over the charge and remelting twelve times in a deep round hearth. The charge was later cast in a long narrow hearth. As-cast bars, 10mm x 10mm x 150mm were lightly deformed then homogenized in vacuum at 1100°C for 150 hours [11]. Homogenized material was rolled to about ten percent reduction, and tensile specimens were machined. The specimens were vacuum annealed at 1100°C for five hours and quenched in ice water. The average grain size at this point was 0.15mm. The elemental composition of as-quenched alloy was determined by measuring the lattice unit cell parameter [7,10,11]. X-ray diffractometer data from bulk samples had lattice parameters which corresponded to compositions [7] of 14 at.% Mo $\pm$ 0.8 percent Mo and 17 at.% Mo $\pm$ 0.8 percent.

To survey the aging response of the alloy, samples were heated in flowing argon and the hardness measured as a function of aging time. Samples 5mm x 10mm x 5mm thick of quenched material were wet ground so that the sample had two sides parallel. After aging, at least 15 indentations were averaged to obtain the hardness value. A Vickers diamond pyramid indenter with 10 Kg load was used.

3.2 Transmission Electron Microscopy (TEM)

Several operations were used to obtain samples of alloy thin enough for TEM. Two millimeter sections were cut from bulk material with a water cooled cut-off wheel. Deformed material was cut at an angle of 45° to the applied stress axis so that more dislocation contrast would be visible in TEM. The 2mm sections were wet ground to 0.006 inch thickness with abrasive paper. Discs 2.3mm diameter were punched from the 0.006 inch section. Samples were further thinned by electrochemical methods [26]. The discs were dimpled to about 0.001 inch thickness with 2:1 H_2SO_4: H_2O solution. 200 volts were applied across a specimen-to-cathode distance of 2.5 cm. Final thinning was via an electrolytic cell containing 2:1 H_2SO_4: H_2O at $0^{\circ}C$ (circulating ice water). Six volts were applied across a specimen-to-cathode distance of two cm.

Suitably thinned samples were examined in a Siemens 1A electron microscope operated at 125 Kv. Sample orientation in the electron beam was varied by means of a Swan tilting stage.

3.3 Quantitative Metallography: Particle Size

An accurate measure of precipitate diameter was needed for the calculation of flow stress in the models of deformation previously discussed (See equations (2), (4), and (5)). The most direct method of measuring particle dimensions was to measure the diameter of a large number of precipitates visible in a suitable TEM micrograph [18]. As discussed in Chapter II, the edge length of cubic Ni_4Mo precipitates was taken to represent the diameter of a spherical Ni_4Mo particle.

The order variants possible in a Ni-Ni_4Mo system should be considered so that a reliable measure of the edge length of a cubic precipitate can be made from TEM micrographs of Ni-Ni_4Mo microstructures. As stated in section 2.2.2, two unique Ni_4Mo variants may nucleate on each {100} fcc. If the variant is nucleated on the (001) fcc of a single crystal of disordered Ni-Ni_4Mo, the resulting cube-shaped precipitate will appear square when seen in a (001) electron microscope reflection. The $(100)_{tet}$ and $(010)_{tet}$ of this Ni_4Mo variant are rotated from the respective fcc matrix directions, and the variant appears rectangular when seen in the (100) and (010) fcc microscope reflections (See Figure 2). The same relationships are true for variants nucleated on the (010) fcc and (100) fcc of this disordered single crystal of Ni-Ni_4Mo. If there is a random mixture of variants in this single crystal, then for a given {100} fcc reflection, one-third of the particles should have a square appearance and two-thirds should have a rectangular appearance (See Table 1).

Since the precipitates were shown by this study to have the morphology and lattice orientation stated in the above paragraphs, it was most convenient to measure particle diameter from {100} micrographs. It was assumed that there was a random distribution of order variants in the alloy, and only the diameters of variants with a square cross section were measured. Unlike spherical particles, it was not necessary to correct such direct measurements from a micrograph of the edge length of cubic particles, since a section of a cubic structure cut parallel to a cube face always represents the

Table 1. Appearance of Order Variants in {100} Micrographs.*

	Matrix Orientation	Appearance of Particles
1	(100)	2, 100 variants: appear square
		2, 010 " : rectangular
		2, 001 " : rectangular
2	(010)	2, 100 " : rectangular
		2, 010 " : appear square
		2, 001 " : rectangular
3	(001)	2, 100 " : rectangular
		2, 010 " : rectangular
		2, 001 " : appear square

*for a random distribution of (100), (010), and (001) variants.

true particle cube edge length.

Precipitate contrast was best seen in dark field micrographs of superlattice (precipitate) spots in a {100} reflection. The presence of strain contrast, due to lattice misfit, in bright field micrographs obscures much of the precipitate constrast in Ni-Ni_4Mo micrographs; however, the strain contrast was not visible if a suitable dark field reflection was selected. Superlattice reflections contained essentially no strain field contrast and produced a sharp particle image on the TEM dark field micrograph.

In order to find the average diameter of a large number of precipitates, an inspection/counting technique was utilized [27]. By visual inspection of the {100} dark field micrographs of 17 at.% microstructures, it could be seen that the particle size distribution was very narrow, and no significant error would be introduced if each of the square particles were placed into one of four diameter classes. A given particle was fitted to one of four circular templates and

counted. For each micrograph, about one hundred precipitates were measured, and the average cube edge length was taken as the particle diameter for that microstructure.

3.4 Yield Stress

For this study tensile tests were conducted on variously aged specimens at room temperature and at elevated temperatures (150°C and 300°C). In both cases a floor model Instron testing machine was used with a testing strain rate of 0.01/min, and the flow stress was determined at 0.2 percent offset. The specimens were pulled to a total strain of three percent. Cylindrical specimens were machined prior to solution treating and aging (gauge sections of 18mm long x 4.5mm in diameter). For the room temperature and 150°C measurements the stress-strain curves were obtained by use of an Instron 0.5 inch strain gauge extensometer. At 300°C the strain was measured by cross-head displacement since the extensometer could not be used at this temperature. Since the crosshead and the extensometer data were in good agreement at the lower temperatures, it was assumed that the crosshead displacement was a reliable measure of strain at 300°C. For the elevated temperature measurements, specimens were pulled in an Instron environmental chamber. Two specimens were tested in each case and the results were found to be reproducible to within ten percent of the yield stress. For the 150°C and 300°C tensile tests, the specimen grip surfaces were threaded so that slip in the grips was minimized.

CHAPTER IV

RESULTS

4.1 Precipitation in Ni-Ni_4Mo Systems

The decomposition of quenched Ni-Mo alloys to a two phase micro-structure was surveyed at different compositions and temperatures to aid in the selection of a microstructure suitable for a precipitation-strengthening study. Alloys of 14 at.% Mo and 17 at.% Mo were examined after aging at 700°C, 750°C, or 800°C. This represented volume fractions of 0.2 (14 at.%, 700°C), 0.3 (17 at.%, 800°C), 0.34 (17 at.%, 750°C), and 0.38 (17 at.%, 700°C). Before aging, the quenched alloys had the short range order, SRO, diffraction pattern of disordered (quenched) Ni_4Mo [5].

The preliminary study of phase separation in these alloys indicated that at 700°C the diffusion kinetics were relatively slow. With a 14 at.% alloy, there was no evidence of precipitates or ordering after 50 hours. No distinct precipitate particles were resolved and the selected area electron diffraction, SAD, patterns displayed no spots which could be attributed to well-developed long range order. The "as-quenched" diffraction patterns persisted for at least 50 hours. 17 at.% Ni-Mo alloy aged ten hours at 700°C (0.4 volume fraction of precipitate) exhibited LRC diffraction patterns, but precipitates were not distinguishable in the alloy by TEM. 17 at.% alloy apparently had a very fine-grained ordered

precipitate dispersion after ten hours at 700°C; the particles were not large enough to be visible by TEM until the alloy was aged 50 hours.

Aging 17 at.% solid solutions at 800°C, and 700°C showed that nucleation of the precipitate phase was markedly dependent on the temperature at which the solid solution decomposed. From electron microscopy studies it was concluded that nucleation was homogeneous below 750°C:

A. At higher temperatures (800°C), heterogeneous nucleation (via grain boundaries, dislocations, vacancies, etc.,) apparently controlled the precipitation of plate-like ordered Ni_4Mo particles (See Figures 6 and 7). Significant hardness increases over that of the quenched state were also recorded (Figure 6). The plate-like particles were approximately parallel to {100}. SAD patterns from {100} reflections had the characteristic pattern of ordered Ni_4Mo [5]. The distribution of precipitates was not uniform, but grain boundary nucleation did not appear to be important since there was no increased concentration of particles at grain boundaries. Since 800°C was near the two phase solvus line (825°C for 17 at.%), the degree of supersaturation during aging at 800°C was low. Low energy nucleation sites at lattice imperfections -- heterogeneous sites -- could have absorbed all the metastable material from the matrix and the resulting precipitate dispersion would have been non-uniform and the particle geometry irregular.

B. At 700°C, the precipitates were nucleated homogeneously, but the precipitate phase consisted of small particles which were

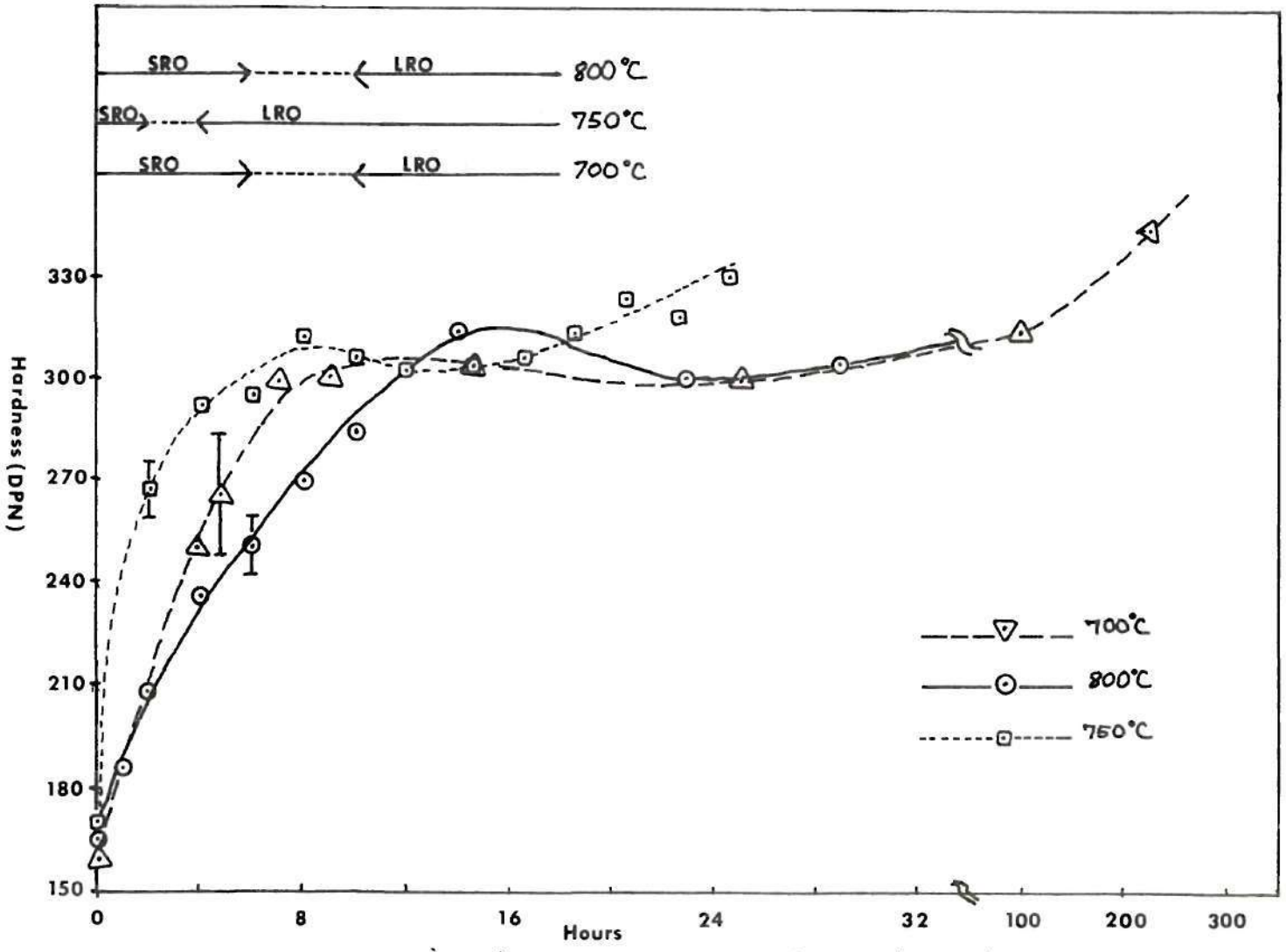

Figure 6. Hardness Versus Aging Time (17 at.% Alloy).

difficult to resolve in the electron microscope. LRO diffraction patterns were observed after ten hours at 700°C, but 50 hours at 700°C were required before distinct particles were visible by transmission. The supersaturation at 700°C aging was larger than the higher temperatures (See Figure 1).

C. At an aging temperature of 750°C, the microstructure was found to be made up of uniformly dispersed precipitates much smaller than those formed at 800°C, but large enough to be resolved in the electron microscope. After four hours at 750°C the presence of LRO was observed in electron diffraction patterns, and a field of cuboidal particles about 300A diameter was seen at {100} matrix orientations. At aging times greater than ten hours, the precipitates often appeared to be aligned in columns when {100} reflections were seen by transmission microscopy. Similar aligned microstructures were observed by Kear et al. in other systems with ordered coherent precipitates and were attributed to the particle coarsening process [28].

These changes in precipitation mode with temperature were consistent with the behavior seen in other systems containing coherent, ordered intermetallic precipitates [1,31,32,33]. In general, as the temperature of aging decreases below the solvus line, the precipitate phase first nucleates heterogeneously on dislocations, grain boundaries, and other imperfections in the lattice of the solid solution. The precipitate morphology is often irregular, and the precipitate dispersion is irregular. At lower temperatures the supersaturation normally increases, and at some level of supersaturation a uniform dispersion of particles is homogeneously nucleated. There may be a

mixture of nucleation modes in the range where there is a transition between nucleation mechanisms [2]. At still lower temperatures, the greater supersaturation leads to increased nucleation density and therefore the microstructure has a finer dispersion of particles.

4.2 Microstructure of 17 at.% Alloy Aged at 750°C

The precipitate particles produced by aging at 750°C were found to be cuboidal in shape with faces parallel to {100} matrix planes. On the basis of the known lattice misfit (0.9 percent) and the observed particle sizes (<500Å) they were assumed to be completely coherent with the matrix. This assumption is consistent with similar calculations of coherency by Brooks and Orowan [23]. The cuboidal shape of the Ni_4Mo particles in this composition range has also been observed by Spruiell [40].

4.2.2 Kinetics of Precipitate Growth

As discussed in Chapter II, the precipitate volume fraction in the 17 at.% alloy is taken to be constant after a few minutes of aging. Therefore during the remainder of the aging process the average particle size increased by particle coalescence. The growth rate of particles due to aging may be seen in Figures 8 and 9. All micrographs in Figure 8 were taken by dark field techniques at {100} matrix orientations. Magnification for all micrographs was 15,000x. The precipitates were often poorly resolved in bright field micrographs of 17 at.% alloy. If one used Ni_4Mo superlattice spots in dark field microscopy the resolution of precipitates was greatly improved. Most of the intensity seen in the dark field micrographs

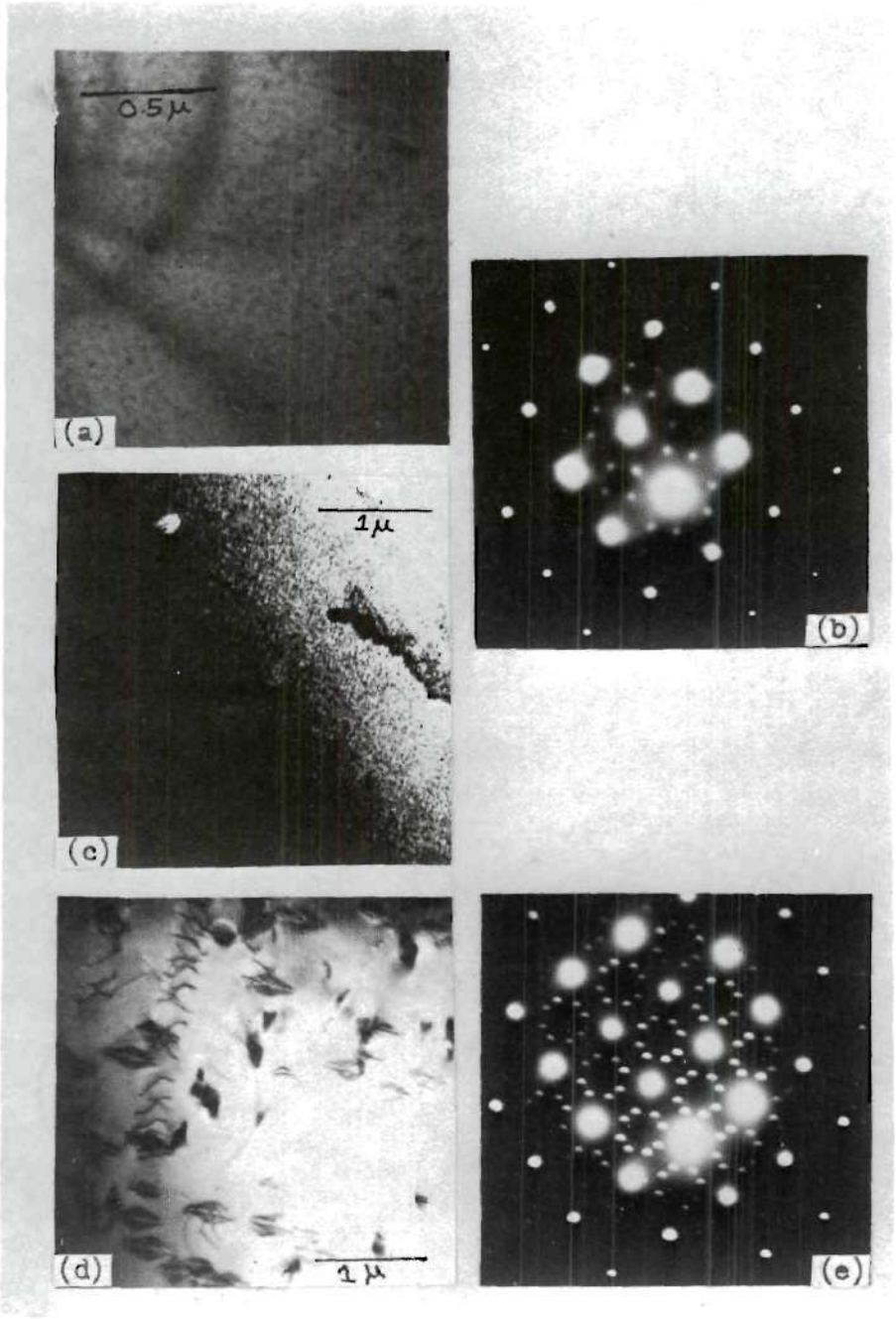

Figure 7. Microstructural Changes Associated with Aging in Ni-Ni_4Mo Alloys. (a) Quenched Alloy. (b) Diffraction Pattern Showing SRO Characteristic of (a) and (c). (c) 14 at.% Alloy Aged at 700°C for 200 Hours. (d) 17 at.% Alloy Aged at 800°C for 10 Hours. (e) Diffraction Pattern Showing LRO Characteristic of (d).

was due to precipitate reflections, and precipitate boundaries were sharply defined.

Particle size was measured according to the methods described in Chapter III. Briefly, dark field micrographs of superlattice reflections were taken at {100} foil orientations. By measurements on enlarged micrographs, an average particle size was found for each aging interval. These average values are shown in Figure 9. The particle growth rate was near the rate reported for precipitates in binary, Ni-base alloys [15].

It is suggested that the experimental hardness curves were a qualitative measure of decomposition kinetics in the 17 at.% solid solution. This could be seen by comparison of the hardness values with the work of Lamp and Stansburg [34]. They found that the ordering rate curve (TTT) of stoichiometric Ni_4Mo was C-shaped with a maximum rate of phase separation near 750°C. The rate of hardness increase in the 17 at.% alloy was greater at 750°C than at 800°C or 700°C (See Figure 6). The precipitate microstructure and diffraction evidence of ordering both supported the view that the solid solution decomposed into two phase material more rapidly at 750°C. It was concluded that at 750°C the diffusion rate and degree of supersaturation together gave a maximum rate of mass transport to sites of precipitate growth.

4.3 Deformation of 17 at.% Alloy Aged at 750°C

4.3.1 Yield Stress

The flow stress increased rapidly for the first four hours.

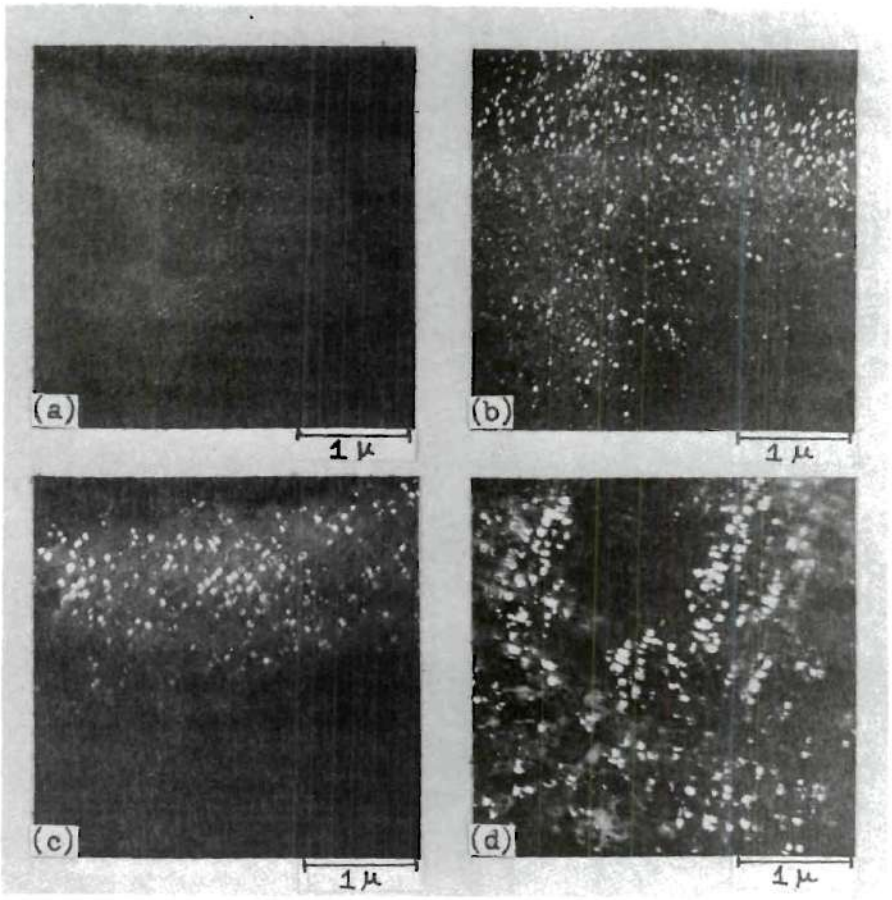

Figure 8. Transmission Microstructures Produced by Aging 17 at.% Alloy at 750°C: Dark Field Micrographs Using Superlattice Spots From (100) Reflections. (a) 1 Hour Aging Time. (b) 3 Hours Aging Time. (c) 16 Hours Aging Time. (d) 59 Hours Aging Time.

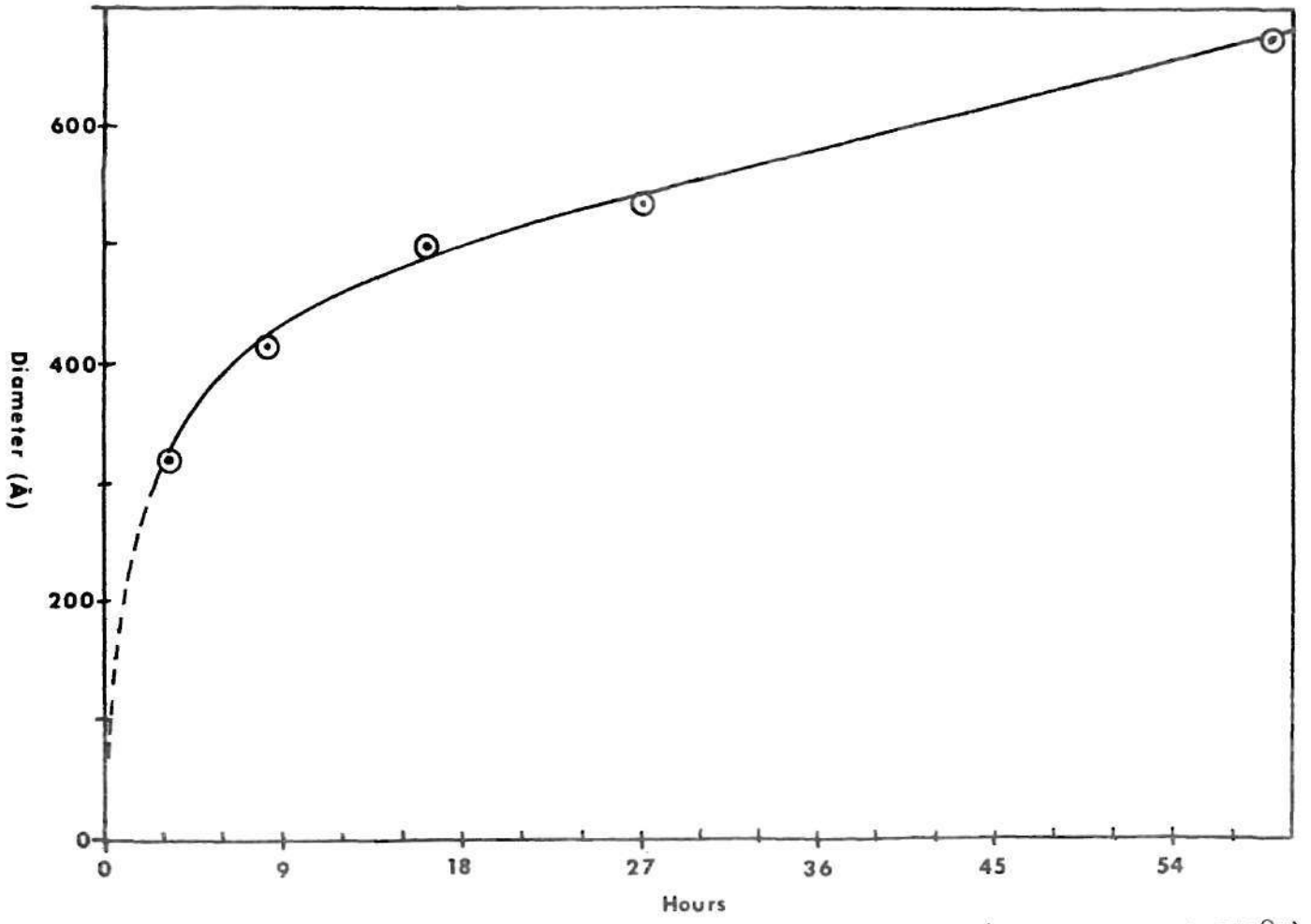

Figure 9. Aging Time Versus Precipitate Diameter. '17 at.% Alloy Aged at 750°C)

This corresponded to the rapid growth of precipitates and to the appearance of long range order (LRO) in the precipitates. The LRO was evidenced by the presence of superlattice reflections corresponding to ordered Ni_4Mo [5]. After four hours, the flow stress increased at a much slower rate which continued for over 50 hours. Since the precipitates were apparently ordered with four hours, further strength increases were attributed to the proven increase in particle size with continued aging. (See Figure 9). Typical stress-strain curves of aged 17 at.% alloy are given in Figure 10. Notice that the work hardening rate and Young's modulus both increased with larger particle size (longer aging time). Yield stress as a function of aging time is shown in Figure 11. The experimental points represent an average of three runs. In tensile specimens which had been aged one hour or more, slip bands were visible on the surface after a three percent deformation. The slip bands formed a coarse pattern (0.1mm between parallel slip lines) of slip lines in a direction about 45 degrees to the stress axis of the specimen.

Since models of precipitate strengthening describe deformation in a single crystal, it was necessary to convert the age-induced yield stress measured from polycrystalline alloy to an equivalent resolved flow stress for a single crystal. The yield stress due to aging, or precipitate growth, was found by subtracting the yield stress of quenched alloy from the total yield stress of an aged alloy. The conversion to an equivalent resolved flow stress is most reliable if one knows the ratio of single crystal to polycrystalline yield stress at some nearby composition. Otherwise a Taylor factor

is used. The Taylor factor approaches 0.33 if the polycrystalline alloy has a very fine grain size and has no preferred grain orientation [35]. Grain size in the 17 at.% alloy was small enough to assure that the measured yield stress was representative of the bulk strength of the alloy; the gauge diameter (3mm) was approximately 20X the grain size (0.15mm). Since the grain size was small and the alloy was deformed no more than 20 percent by rolling, no significant fraction of preferred orientation should have been present in the tensile specimens [39], and the Taylor factor of 0.33 was appropriate for converting the aged-induced yield stress of 17 at.% to an equivalent resolved flow stress. The resolved flow stress for 17 at.% Ni-Mo is shown on Figures 16 and 17. Also shown for comparison are the limits [35] of flow stress which could occur for a fcc metal if the alloy had strong preferred orientations. It may be seen that the choice of a specific Taylor factor would not drastically shift the level of flow stress relative to the theoretical curves. Note that the experimental flow stress is a linear function when plotted against the square root of particle radius. This is typical behavior for precipitation strengthened alloys [23].

The temperature dependence of yield stress was found to be small, but the data (See Figure 12) showed a consistent downward trend with increasing temperature which suggested that some coherency strain strengthening was present. From changes in the Young's modulus and the flow stress with temperature, Oblak found evidence that the flow stress of an alloy with large coherency strains was directly proportional to the shear modulus G [18]. This relationship between

strength and G is predicted by coherency strain models of precipitation hardening (See Chapter II). Similar evidence for coherency strain strengthening was found from study of 17 at.% Ni-Mo. The flow stress data in Figure 11 were fitted to a linear curve with slope (M_2) of -0.08 $Kg.mm^{-2}.{}^{o}C$. Since G is directly proportional to Young's modulus E (assuming Poisson's ratio is constant), the slope of ($E_T/E_{25^{o}C}$) versus temperature, is equal to the slope of ($G_T/G_{25^{o}C}$) versus temperature. A graph of ($E_T/E_{25^{o}C}$) versus temperature, over the range of 25°C to 150°C, had a slope (M_1) of $-0.00176^{o}C^{-1}$. If the flow stress (Figure 12) is directly proportional to the modulus, then the temperature coefficient of flow stress (M_2) should be directly proportional to the temperature coefficient (M_1) of the modulus. The product of M_1 times the yield stress at 25°C is -0.084 $Kg.mm^{-2}.{}^{o}C^{-1}$, in good agreement with the temperature coefficient of the flow stress.

4.3.2 Slip Bands in Deformed Ni-Ni_4Mo

The characteristic microstructure of deformed 17 at.% Ni-Mo was observed to change with aging. The quenched alloy deforms via closely spaced {111} slip bands, and also by secondary dislocations which appear to slip in {111} (See Figure 13). Aging for one to five hours caused slip to be more localized; most dislocations were confined to broad bands where the dislocations were seen moving in planar arrays (See Figure 13). At larger particle sizes -- aging times of ten hours or more -- slip bands were less numerous in the alloy and the band width was narrower (See Figure 14). By trace analysis, it was shown that the bands at various aging times were all

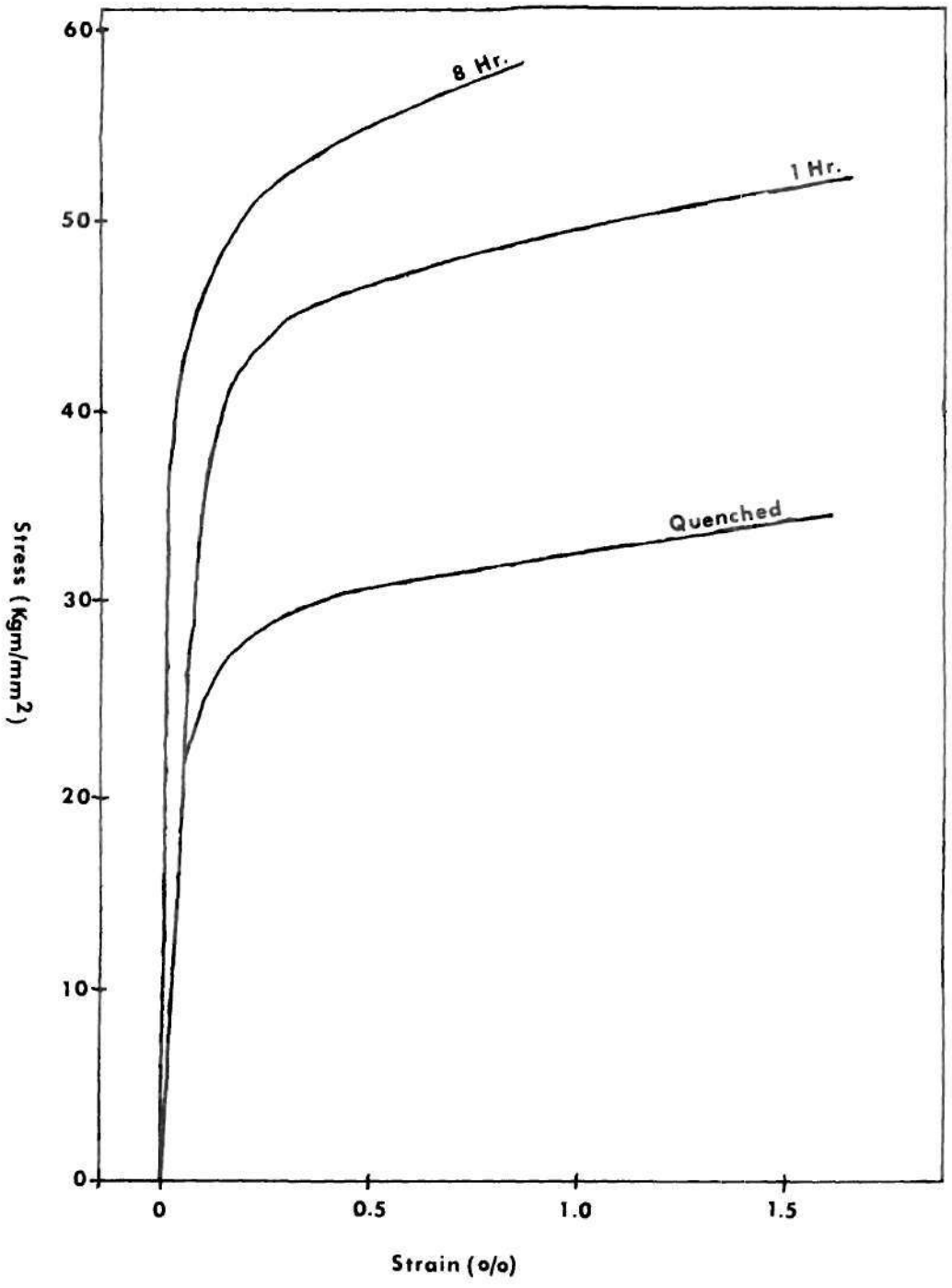

Figure 10. Stress-Strain Curves at 25°C Showing the Effect of Aging Time at 750°C after Quenching from 1100°C. (17 at.% Alloy)

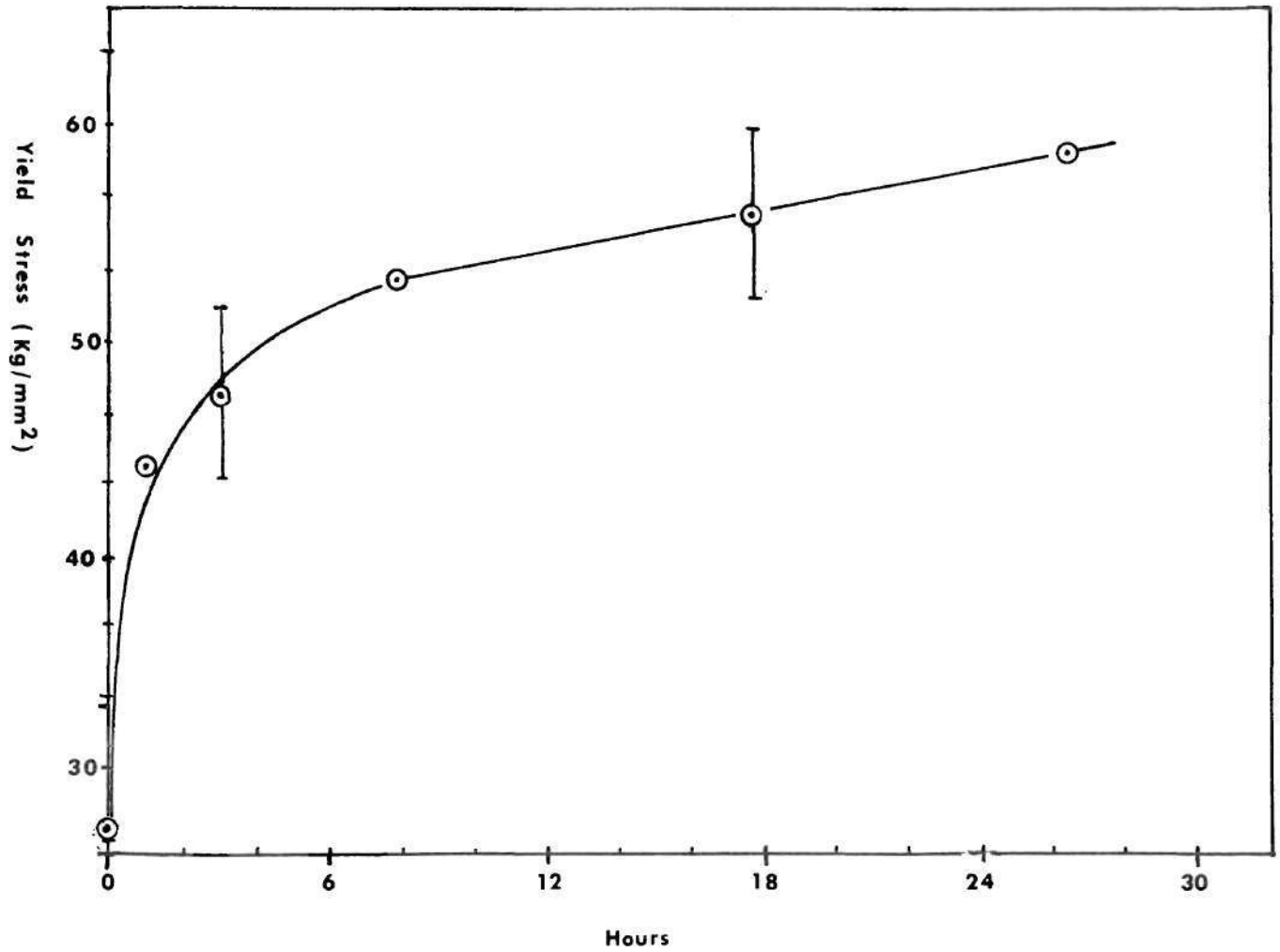

Figure 11. Yield Stress Versus Aging Time. (17 at.% Alloy Aged at 750°C)

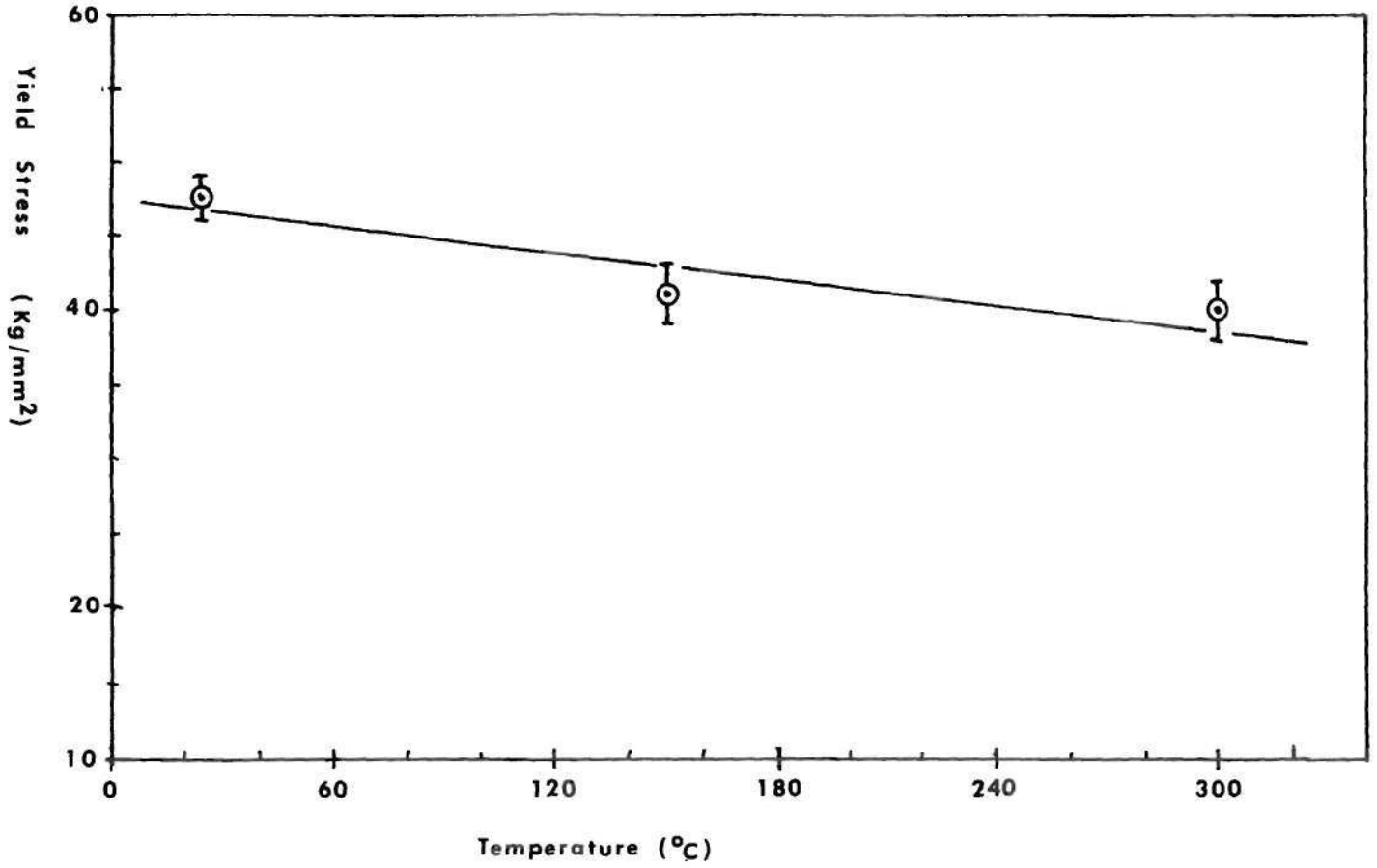

Figure 12. Temperature Dependence of Yield Stress. 17 at.% Alloy Aged for Three Hours at 750°C.

parallel to {111} of the matrix of 17 at.% alloy.

4.3.3 Precipitate Shearing

Some direct evidence of precipitate shearing in 17 at.% Ni-Mo may be seen in Figure 15. Due to the strain field contrast around the precipitates and the high density of particles in the alloy, it was difficult to tilt the specimen so that dislocation contrast was visible when particles were also visible. In Figure 15 there is a large offset in the particle which could be attributable to multiple shears, or to breakage of the particle during deformation.

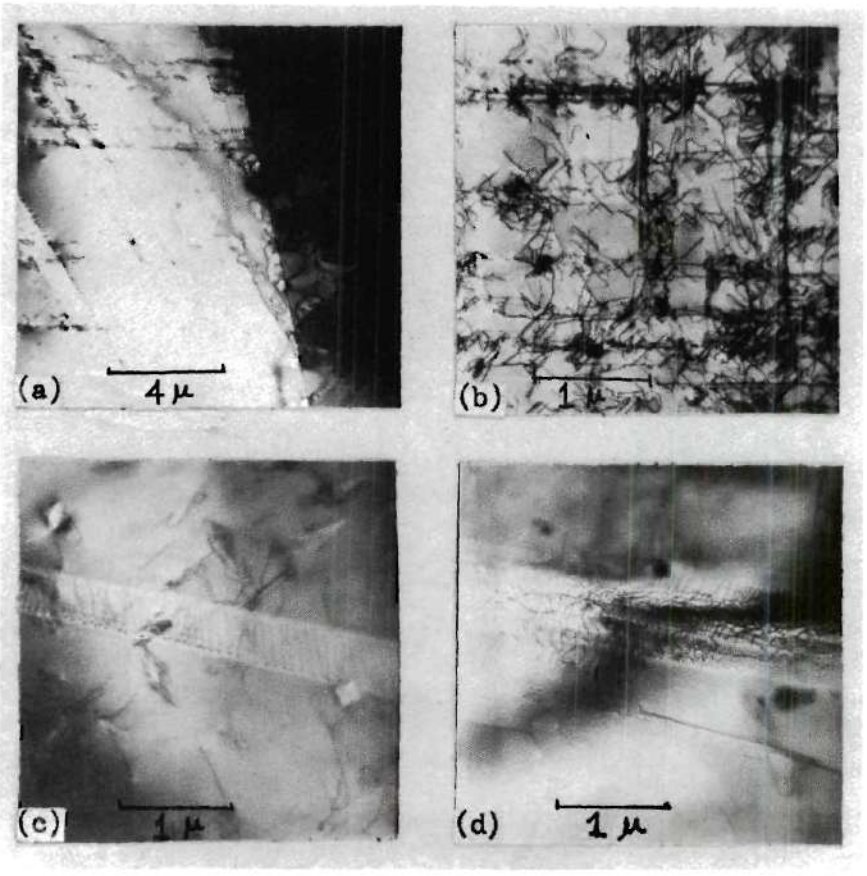

Figure 13. Slip Bands Observed in 3% Deformed 17 at.% Ni-Mo Alloy. (a) Quenched Alloy. (b) Quenched Alloy. Reflection from (100). (c) and (d) Alloy Aged for Five Hours at 750°C.

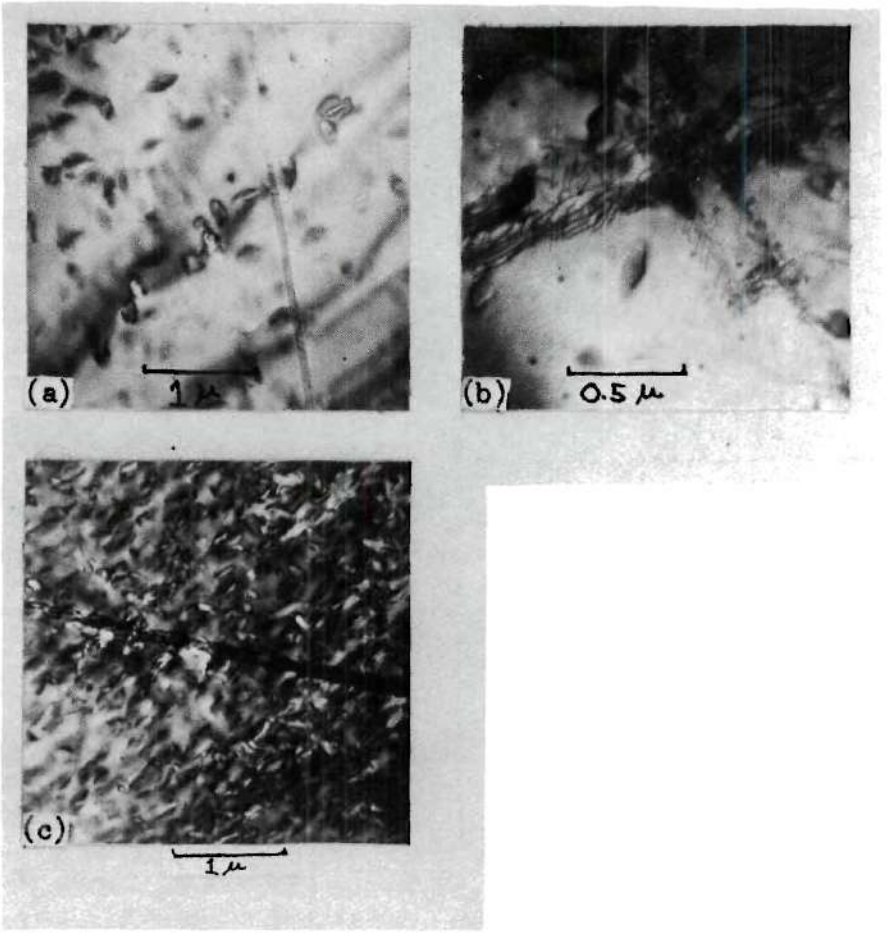

Figure 14. Slip Bands Observed in Deformed (3%) 17 at.% Ni-Mo Alloy. (a) and (b) Alloy Aged for Five Hours at 750°C. (c) Alloy Aged for 18 Hours at 750°C.

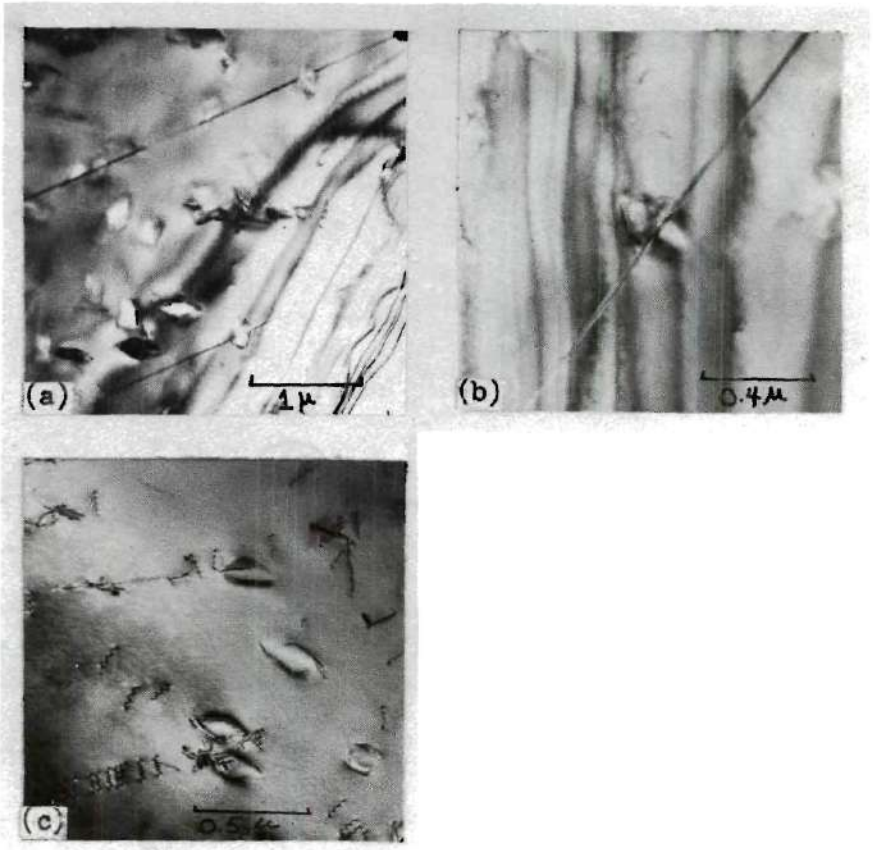

Figure 15. Evidence of Precipitate Shearing in Transmission Microstructures. 17 at.% Ni-Mo Aged at 750°C and Deformed Three Percent. (a) and (b) Alloy Aged for Three Hours. (c) Alloy Aged for Five Hours.

CHAPTER V

DISCUSSION OF RESULTS

There were several reasons why the microstructures produced by aging 17 at.% at 750°C were suitable for a study of precipitate strengthening. The alloy contained a dispersion of particles which could reasonably be expected to strengthen the alloy by impeding the movement of glide dislocations. The particles were sufficiently large so that particle/dislocation interactions could be clearly resolved in transmission microscopy. The particles were uniformly dispersed and reasonably equi-axed. There was an interval in the aging process where the particle diameter increased at a slow uniform rate so that particle size could be related to flow stress with confidence. The particles were apparently highly ordered after a short aging time (four hours), since LRO diffraction intensity was uniform across the micro-structure after four hours. The flow stress study was confined to short aging times (four to 27 hours) so that particle size was as small as possible. Generally, smaller particles are more effective in precipitate strengthening of an alloy, so within the limits of the system -- 17 at.% Ni-Mo aged at 750°C -- the microstructures having the smallest uniform precipitate dispersion were investigated.

The relative importance of particle order, particle misfit, and Orowan processes are now discussed in sequence. Other possible strengthening effects due to aging -- surface energy and modulus

effects -- were taken to be negligible (See Chapter II). The APB, misfit, and Orowan models were independently compared to the experimental properties of 17 at.% Ni-Mo, since the author was not aware of any treatment which quantitatively accounted for the behavior of an alloy in which several mechanisms were simultaneously operating.

In order to make quantitative predictions of flow stress for a specific alloy, several variables in equations (2) through (5) must be measured experimentally or a reasonable value must be calculated or assumed. The need for accurate parameters must be emphasized. Ideally, a deformation model would accurately predict the absolute value of the flow stress. However, since it was beyond the scope of this study to measure all the variables required for the flow stress calculation, a considerable margin of error is present in the flow stress predictions. For example, the APB energy at 25°C was estimated from a theoretical expression, and no estimate was available for the temperature dependence of this parameter.

For the purposes of this study, the shear modulus, G, was derived from experimental data (See Appendix A). As discussed in Chapter II, one-half the edge length of cubic Ni_4Mo precipitates was taken to be equivalent to the average radius, r_s, of spherical Ni_4Mo particles. The volume fraction of precipitate, f, was taken to be the equilibrium phase distribution at 750°C. The Burger's vector, b, was 2.5A, assuming that a/2 [110] (111) dislocations accounted for all strain in the alloy. Since extensive faulting was not seen in the deformed samples, the assumption of a/2 [110] dislocations was probably justified for this alloy. The APB energy, γ, was found

using Chakravarti's expression [10] for APB formed by slip on {111} in ordered Ni_4Mo (See Appendix C). The lattice misfit parameter, ϵ, was calculated as described in Chapter II. If all dislocations are assumed to be straight, the line tension, T, equals $Gb^2/2$. This value for line tension was appropriate because the particle volume fraction was relatively large and the particles were small ($\leq$ 500A) so that the interparticle spacing was of the order of particle diameter. Bending of dislocations between the closely spaced particles would be a high energy process. Although some degree of bending probably occurred, particularly at the first unit of the superdislocations, the precipitate density and observed dislocation geometry both justified use of the above equation for line tension.

The Ni_4Mo particles were sheared during deformation, rather than bypassed via the Orowan mechanism. There were several reasons for this conclusion. First, the volume fraction of precipitate phase was nearly 40 percent. This meant that the particles were closely spaced and dislocations had to bend to a sharp radius of curvature in order to move between the particles. In Figure 16, it can be seen that the experimental flow stress increased with precipitate size while the Orowan theory predicted a decrease. Assuming a square lattice spacing of precipitates and a precipitate diameter of 500A, the calculated precipitate spacing is 200A. The critical stress for Orowan looping at this particle spacing was about 90 Kg/mm^2. The experimental flow stress was about 10 Kg/mm^2. If the 17 at.% alloy were deforming by an Orowan mechanism, the precipitates would have been more than 2000A in diameter, (See Appendix B for

calculations). In many systems, an aged alloy shows an increase in the work hardening rate, compared to the solid solution, if an Orowan mechanism occurs. But the work hardening rate is relatively unchanged if precipitates are sheared during deformation [23]. The small change in work hardening rate in Figure 11 thus suggested that the precipitates were sheared when 17 at.% Ni-Mo was deformed.

The order strengthening models, equations (2, 2d, 2e, 2f) and (4), (using variables discussed in preceeding paragraphs) are shown in Figure 16 (See Appendix D for calculations). It is apparent that the deformation of 17 at.% Mo was not controlled by single dislocation shearing of ordered Ni_4Mo particles. This result is in good agreement with the analysis made in Chapter II. The five dislocation model of order hardening differs from the experimental data by about 40 percent. Since the slopes of the curves are similar, and the absolute values are close, an order strengthening model with five-unit superdislocations gives a good account of the observed flow stress of 17 at.% Ni-Mo. As discussed in Chapter II, and as shown in Figure 16, the decreasing flow stress of two, three, four or five dislocation geometries on the slip plane means that glide dislocations could tend to "pile up" until the five dislocation geometry was attained. One would expect to observe a distribution of superdislocation configurations at small strains; these would approach a five-unit geometry as the lattice strain increased. As pointed out in Chapter IV, dislocation contrast was difficult to isolate from precipitate and strain field contrast in TEM studies of 17 at.% alloy. In the dislocations observed, groups of two or

more parallel dislocations were frequently seen on {111}. Such observations support the superdislocation order strengthening models.

The Gerald and Haberkorn model of coherency strain strengthening (equation 5) was used to predict the alloy flow stress using the variables discussed in preceding paragraphs. Several curves of $(\Delta\tau)$ versus $r_s^{1/2}$ were calculated by assuming values for the misfit parameter ϵ (See Appendix E). These curves are shown in Figure 17. The curve corresponding to the average misfit of particles in 17 at.% Ni-Mo (0.75 percent misfit) was much higher than the experimental strength, but the theoretical slope (i.e., the particle size dependence) was similar to that of the experimental flow stress. Since the predicted flow stress was much too large, it is possible that an accurate spherical misfit value could not be calculated for the 17 at.% alloy by averaging the absolute values of orthogonal lattice misfit parameters. The compressive and tensile stress fields around the Ni_4Mo particles may tend to cancel so that the effective spherical misfit parameter is smaller than 0.75 percent.

There was close agreement between the stress predicted by the five-dislocation model of order hardening and the experimental flow stress; moreover, the order prediction was calculated with less uncertainty than was the coherency strain prediction. The expressions for flow stress due to order and misfit strain differ only in their dependence on G, APB energy, and misfit parameter ϵ. Since G was accurately determined from experimental data (See Appendix A), there was little error due to G. The APB energy value was based on the Bragg-Williams model and has given reliable values for other alloys

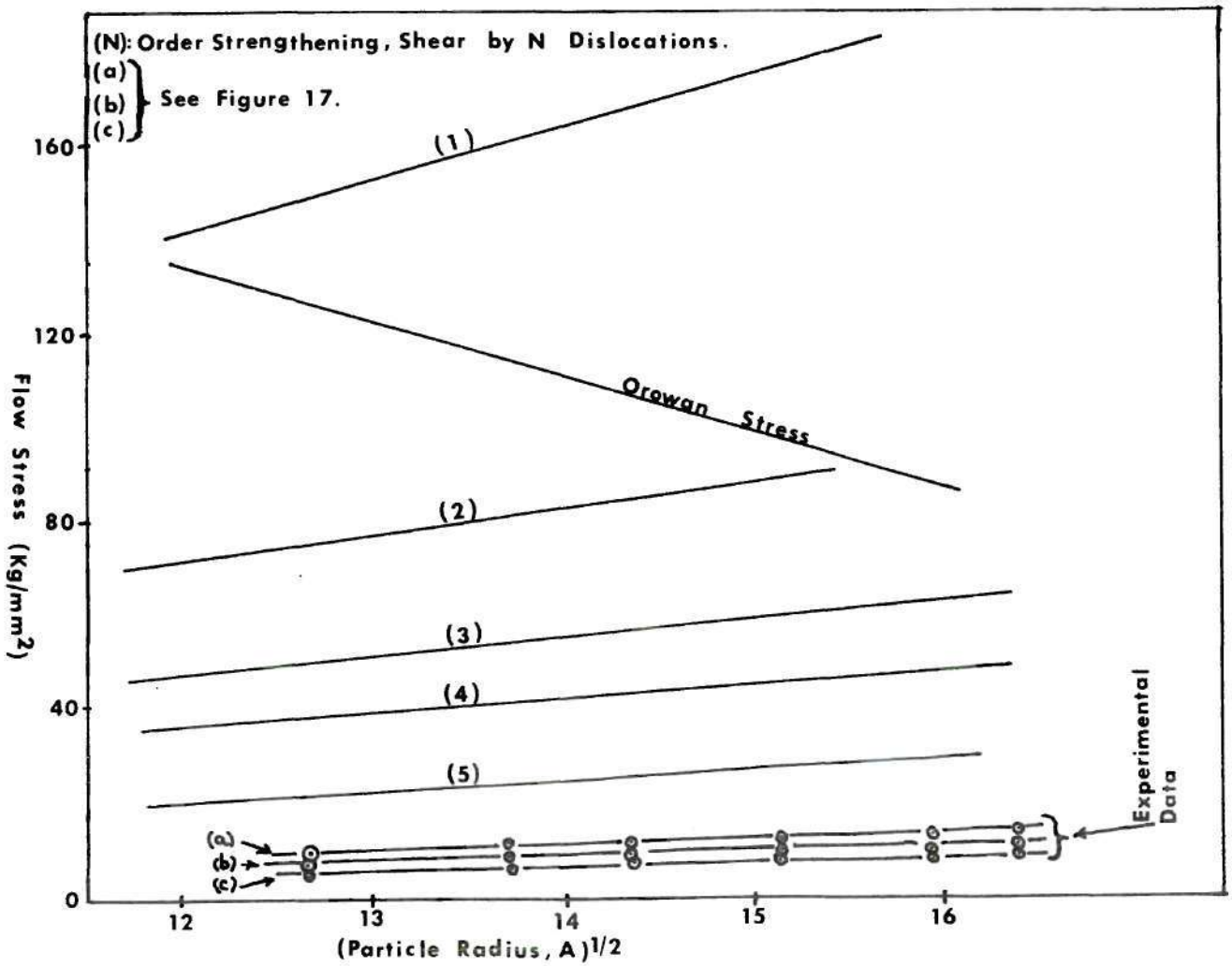

Figure 16. Comparison of Flow Stress Predicted by Orowan and Order Strengthening Models with Experimental Results.

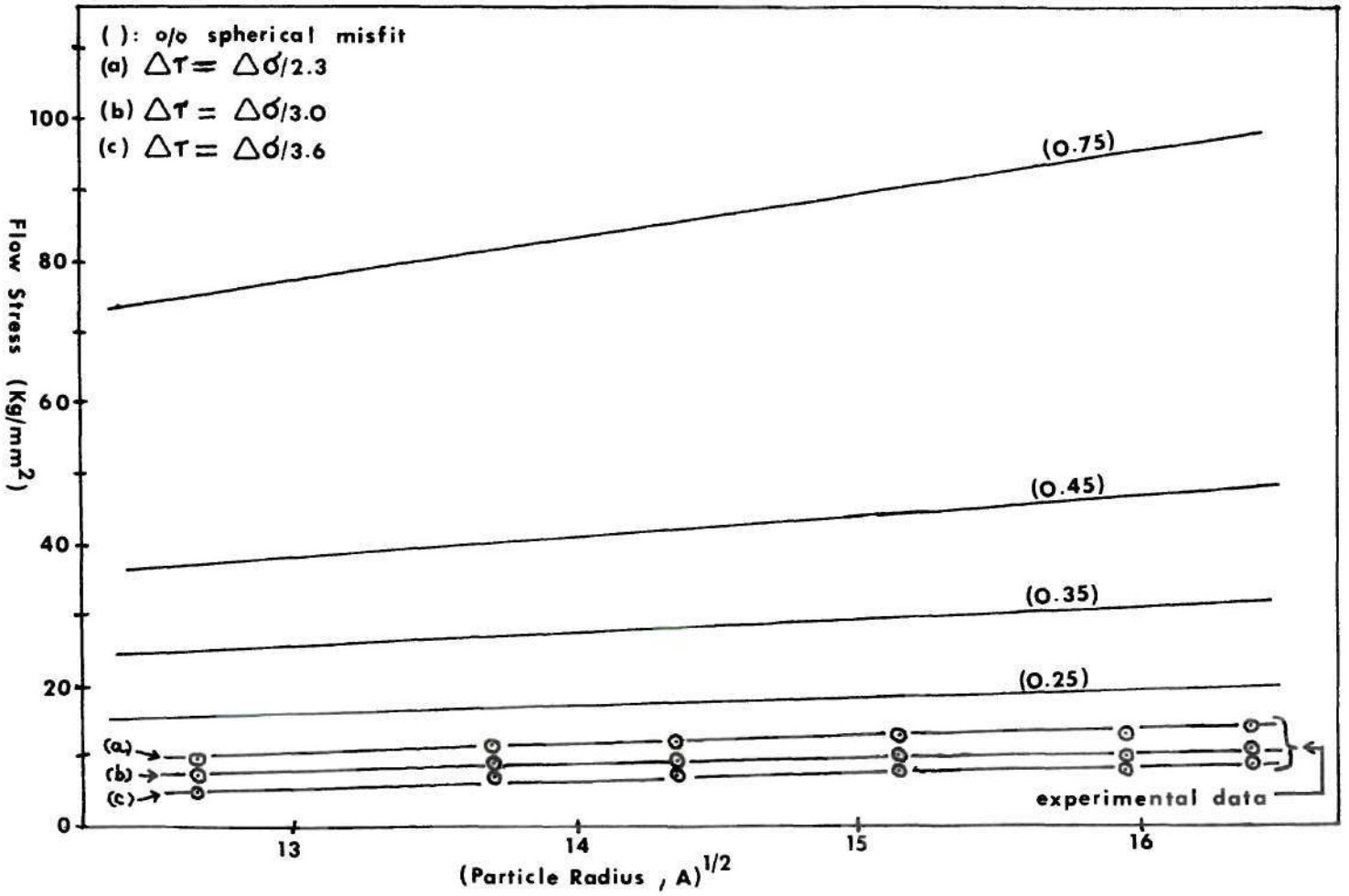

Figure 17. Comparison of Flow Stress Predicted by Coherency Strain Models with Experimental Results.

[15,20]. In contrast, considerable uncertainty exists about the magnitude of the misfit parameter ϵ which was used to calculate the flow stress induced by misfit. The uncertainly in ϵ was due to the theoretical difficulties in converting the three lattice misfit values of cubic Ni_4Mo particles to a single equivalent spherical misfit parameter for spherical particles.

The coherency strain calculation did not accurately predict the flow stress, but the temperature dependence of flow stress, "strain contrast" visible in TEM, and the known precipitate lattice misfit [7] all indicated that coherency strains contributed to the strength of aged 17 at.% Ni-Mo. As shown in Chapter IV, the temperature coefficient of flow stress was directly proportional to the temperature coefficient of the shear modulus. Such a dependence was predicted by equation 5 (See section 2.4.2), and was shown by a previous study [18] to indicate the presence of coherency strengthening. The fact that the alloy had a temperature dependent flow stress characteristic of misfit hardened systems did not preclude the presence of order hardening. If both mechanisms were operating, the order and misfit components would be proportional to γ/G and G respectively. Both γ and G have an inverse temperature dependence. but since γ is zero at about 800°C, while the alloy melts (G = 0) at about 1500°C, γ may be expected to decrease faster than G. The order component therefore could reasonably have a very small temperature dependence, and only the misfit component would appear when the temperature coefficient of alloy flow stress was measured.

The preceding paragraphs point out that there was evidence of

both order hardening and strain hardening in the 17 at.% alloy. However since quantitative models for multiple deformation mechanisms were not available, no effort was made to determine the relative contributions of order and misfit to the alloy strength.

In summary, the experimental flow stress was in agreement with an order strengthening model based on five-unit superdislocations. However, there were indications that coherency strains were responsible for a fraction of the strength of 17 at.% Ni-Mo. Coherency strain contrast was visible by TEM of aged alloy, a significant lattice misfit was calculated from data of previous studies, and the temperature dependence of flow stress indicated that strain field influence was detectable in the strength of the material. Therefore, both order and coherency strain hardening were present in the alloy. The relative or absolute contributions of these mechanisms to alloy strength could only be determined if the APB energy, shear modulus, and effective misfit parameter were known with much greater accuracy.

CHAPTER VI

CONCLUSIONS

1. Ni-Ni_4Mo aged to produce cuboidal particles in the size range of <500A and with volume fraction of 0.35 Ni_4Mo has been found to deform by planar slip on {111} by shearing the Ni_4Mo particles.

2. The variation in flow stress with particle size (with constant volume fraction) varies linearly with $r_s^{1/2}$ where r_s is the average particle radius. This form is in agreement with predictions of both order hardening models (creation of APB by shear) and strain hardening models. The order hardening model shows the best absolute value agreement with experiment; however, it is felt that this is in part due to the necessary approximations in the lattice misfit parameter and particle geometry.

3. The flow stress was found to vary inversely with temperature at the same rate as does the shear modulus. Since strain hardening is proportional to G, this indicates that coherency strains contribute to the overall strength of the alloy. Order hardening cannot be eliminated on this basis since it depends inversely on modulus and directly on APB energy which decreases with temperature.

4. The relative contributions of order and misfit strain cannot be determined on an absolute basis without accurate values of APB energy and shear modulus as a function of composition and temperature.

APPENDIX A

EXPERIMENTALLY-DERIVED VALUE FOR SHEAR MODULUS (G) IN 17 AT.% ALLOY

Young's modulus for one hour aging at 750°C = 24,000 Kg/mm^2. (from the elastic slope of stress-strain curves measured with an extensometer).

Since $G = E/(2(1 + v))$, and since v is relatively constant at about 1/3 for most materials, v may be taken as a linear function of alloy composition.

$$\left.\begin{aligned} v_{Ni} &= 0.276 \\ v_{Mo} &= 0.305 \end{aligned}\right\} \text{ Hirth [37]}$$

$$v_{17\ at.\%} = 0.280$$

Thus $G = 2.4 \times 10^4/2(1 + v) = 0.9 \times 10^4\ Kg/mm^2$

$$= 0.9 \times 10^{10}\ NM^{-2}$$

Note that $G_{Ni} = 9.9 \times 10^{10}\ NM^{-2}$, [37].

The experimental value of G is lower than might be expected from extrapolation of the modulus of the alloy components, but the experimental value is in good agreement with two other independent researches on Ni-Mo alloys that are near the 17 at.% composition:

(A) Chakravarti [10] found that Young's modulus for 20 at.% Ni-Mo was: $E = 2.11 \times 10^6\ Kg/cm^2$ ($= 2.11 \times 10^4\ Kg/mm^2$). This gives $G = 1.0 \times 10^{10}\ NM^{-2}$, which is very near the value found in this study.

(B) From the stress-strain curves for aged 20 at.% Ni-Mo [25], a value of $E = 3.5 \times 10^7$ psi is measured. This is equivalent to $E = 2.5 \times 10^4$ Kg/mm^2. Using $G = E/2(1 + \nu)$, $G = 1.0 \times 10^{10}$ NM^{-2}. These three independent results strongly suggest that the value $E = 2. \times 10^4$ Kg/mm^2 is a reliable value for this alloy. If Poissan's ratio is about 1/3 for this alloy, then $1. \times 10^4$ Kg/mm^2 is an accurate value for G.

APPENDIX B

CRITICAL OROWAN STRESS

The minimum stress for Orowan looping may be found from the following equation [24]:

$$\tau_c = \frac{0.83Gb \ln[2R_s/r_o]}{2\pi(1-v)^{1/2}L} \qquad \text{(B-1)}$$

where R_s is the effective particle radius, r_o is the diameter of the dislocation "core", L is the square planar spacing of precipitates on the slip plane. v is Poissan's ratio. Equation (B-1), a modification of Orowan's original equation for dislocation looping [41], considers the effects of dislocation loop configuration (the loop is elliptical) and the effects of the interaction of bowed segments of dislocation on the dislocation line tension. The equation takes into consideration the presence of both edge and screw components in the looping dislocation. The factor 0.83 is due to the assumed random spatial distribution of particles on the slip plane [42].

For a random dispersion made up of identical spherical particles with radius R, the mean radius, R_s, of circular section in any plane is $(2/3)^{1/2}R$. Where L is the square lattice spacing of a planar array of particles and N_a is the density of particles in the planar array [15], $L = (N_a)^{-1/2}$. Also, $N_a = f/\pi R_s^2$. Thus, $L = (\pi/f)^{1/2}$. Allowing for finite particle size,

$$L = (N_a)^{-1/2} - 2R_s = R_s[(\pi/f)^{1/2} - 2]$$

Substituting into equation (B-1) and using $(2/3)^{1/2}R$ for R_s and b for r_o, where b is the Burger's vector, yields:

$$\tau_c = \frac{0.83Gb\ln[(2(2/3)^{1/2}R)/b]}{2\pi(1-v)^{1/2}(2/3)^{1/2}R[(\pi/f)^{1/2} - 2]} \qquad \text{(B-2)}$$

In using equation (B-2), it is assumed that the Ni_4Mo precipitates are spherical and that a Orowan strengthening mode is the only source of age strengthening in the alloy. The flow stress of an Orowan mechanism in 17 at.% Ni-Mo was predicted by using the following values:

v = 0.28 (linear combination of v_{Ni} and v_{Mo} [37])

R = 1/2 edge length of Ni_4Mo cubic particles

f = 0.35, from [15]

$G = 0.9 \times 10^{10} NM^{-2}$ (APPENDIX A)

b = 2.54 A, from a/2[110](111) for 17 at.% Ni-Mo [15].

The calculated values are given below.

R(A)	τ_c
144	134 Kg/mm^2
169	119 "
196	107 "
225	97 "
256	87 "
1000	29 "

APPENDIX C

APB ENERGY OF ORDERED Ni_4Mo

Chakravarti [10] has derived the following expression for APB energy of ordered Ni_4Mo:

$$\gamma = \frac{k\,\bar{v}}{a_o^2}$$

where k is a function of the Ni_4Mo plane on which the APB occurs, $\bar{v}$ is the average energy per wrong bond created by APB formation, and a_o is the lattice parameter of Ni_4Mo solid solution. This equation considers the thermodynamics of only nearest-neighbor interactions between atoms on the ordered lattice. APB energy is taken to be the energy of "wrong" bonds formed when atoms slip away from ordered positions.

Using 0.37 for k for (111) slip (10), 14×10^{-14} erg/cm^2 for $\bar{v}(10)$, and a_o = 3.6080 A (7),

$$\gamma = 39.7 \text{ erg/cm}^2 = 39.7 \times 10^{-3} \text{ J/M}^2$$

APPENDIX D

CALCULATION OF ORDER STRENGTHENING IN 17 AT.% Ni-Mo

As discussed in Chapter II, the flow stress due to ordered precipitates may be predicted from the models of Castagne [17] and Ham [15,45]. These order hardening models assume that the material has a dispersion of identical spherical particles which randomly intersect the slip plane. For any system, the predicted shear stress required to move an edge dislocation is twice the stress needed to move a screw dislocation. Therefore, in this study and others [15,18] it was assumed that the flow stress was controlled by edge dislocations.

In applying the order models to the 17 at.% Ni-Mo alloy, it was assumed that the deformation behavior of cubic Ni_4Mo particles closely approximated [15] the deformation of spherical, ordered particles. The dislocation line tension was taken to be $1/2Gb^2$; i.e., it was assumed that the dislocations curved only slightly as they sheared through the precipitate particles.

(A) Shear by Single Dislocations.

The flow stress for a single dislocation which shears the slip plane, of an alloy containing ordered particles is [17]:

$$\Delta\tau_1 = (\gamma/b)[4\gamma f r_s/\pi T]^{1/2} \qquad \text{(D-1)}$$

Substituting for T,

$$\Delta\tau_1 = (\gamma/b)[8\gamma f r_s/\pi G b^2]^{1/2} \qquad \text{(D-2)}$$

For 17 at.% Ni-Mo the following values were used in equation (D-2):

T, average dislocation line tension, $= Gb^2/2$

γ, APB energy, $= 39.7 \times 10^{-3} J \cdot M^{-2}$ (APPENDIX B)

b, Burger's vector, $= 2.54 \times 10^{-10} M$ (APPENDIX B)

f, volume fraction, $= 0.35$ (APPENDIX B)

G, shear modulus, $= 0.9 \times 10^{10} NM^{-2}$ (APPENDIX A)

r_s, particle radius, = 1/2 edge length of Ni_4Mo precipitates.

The following values are calculated for single dislocations:

r(A)	$\Delta\tau_1$	
144	139.	Kg/mm^2
169	151	"
196	163	"
225	174	"
256	186	"

(B) As may be seen from equations 2d, 2e, and 2f, the flow stress (assuming other parameters do not change) for 2-, 3-, or 4-unit superdislocations is equal to the flow stress of a single dislocation (See section A above) divided by 2, 3, or 4 respectively. The flow stress calculated in this way is given below.

r_s(A)	Flow Stress of Paired Dislocations	Flow Stress of Three Dislocations	Flow Stress of four-unit super-dislocations
144	70. K_g/mm^2	46. K_g/mm^2	35. K_g/mm^2
169	76.	50.	38.
196	82.	54.	41.
225	87.	58.	44.
256	93.	62.	47.

(C) Shear by Five-Unit Superdislocations.

The flow stress for a five-unit superdislocation which shears the slip plane of an alloy containing particles with the atomic stacking of ordered Ni_4Mo (equation 4, APPENDIX F) is:

$$\Delta\tau_5 = (\gamma/5b)[(4\gamma f r_s/\pi T)^{1/2} - f] \qquad (D\text{-}3)$$

Substituting for T,

$$\Delta\tau_5 = (\gamma/5b)[(8\gamma f r_s/\pi G b^2)^{1/2} - f] \qquad (D\text{-}4)$$

The variable names and values were those used to calculate one-dislocation flow stress.

r_s(A)	$\Delta\tau_5$
144	20. Kg/mm^2
169	22. "
196	24. "
225	27. "
256	29. "

APPENDIX E

CALCULATION OF COHERENCY STRAIN STRENGTHENING IN 17 AT.% Ni-Mo

As discussed in Chapter II, for an alloy strengthened by matrix/precipitate lattice mismatch, the minimum stress required to produce shear of the material (Gerald and Haberkorn, [19]) is:

$$\Delta\tau = 3G\,(\varepsilon)^{3/2}(r_s f/b)^{1/2} \qquad \text{(E-1)}$$

where G is the shear modulus, ε is the lattice misfit parameter, r_s is the particle diameter, f is the volume fraction of particles, and b is the Burger's vector. The Gerald/Haberkorn model assumes a random dispersion of identical spherical particles on the slip plane. Equation (E-1) assumes that edge dislocations account for all the flow stress. The fact that edge dislocations are of primary importance was treated theoretically at some length by Gerald and Haberkorn [19]. For screw dislocations, the constant (3) in equation (E-1) becomes (1), and the rest of the expression is unchanged.

Gleiter [43,44] has derived a similar expression for the flow stress due to misfitting precipitates:

$$\Delta\tau = 11.8\ G\,(\varepsilon)^{3/2}(r_s/b)^{1/2}(f)^{5/6} \qquad \text{(E-2)}$$

Equations (E-1) and (E-2) do not differ greatly in magnitude of predicted flow stress for a given microstructure, although (E-2) has a greater dependence on f. The deformation models represented by

these equations are currently the subject of controversy, and equation (E-1) was adopted in this study as being more widely accepted at present [15,18].

In applying (E-1) to the 17 at.% Ni-Mo alloy, it was assumed that the deformation behavior of the cubic Ni_4Mo particles closely approximated the deformation behavior of spherical particles with a spherical misfit. Since particles in 17 at.% alloy had misfit of -.46 percent, +.9 percent, and +.9 percent in orthogonal matrix directions, the absolute value of Ni_4Mo misfit was averaged for the three directions to obtain a reasonable value for the spherical misfit parameter required in equation (E-1). The flow stress due to coherency strains in 17 at.% alloy were predicted using the following values:

$G = 0.9 \times 10^{10}$ N/M^2 (APPENDIX A)

f = as used in APPENDIX D

r_s = as used in APPENDIX D

b = as used in APPENDIX D

ϵ = 0.75 percent (average of .45 percent, .9 percent, and .9 percent) (See Section 2.1)

For average misfit (ϵ) of 0.75 percent,

r_s(A)	$\Delta\tau$
144.	71. Kg/mm^2
169.	77. "
196.	83. "
225.	89. "
256.	95. "

By assuming values of (ϵ), the following curves are calculated:

r_s(A)	$\Delta\tau$, ϵ = 0.45%	$\Delta\tau$, ϵ = 0.35%	$\Delta\tau$, ϵ = 0.25%
144	34. Kg/mm^2	23. Kg/mm^2	14. Kg/mm^2
169	37. "	25. "	15. "
196	40. "	27. "	16. "
225	43. "	28. "	17. "
256	46. "	30. "	18. "

APPENDIX F

ORDER STRENGTHENING WHEN SHEAR TAKES PLACE BY GROUPS OF a/2 [110] DISLOCATIONS:

(A) For five dislocations [18, 15], a static force balance at yield may be expressed by the following equations:

dislocation 1,

$$\Delta\tau b + K \sum_{J>1} \frac{1}{d1j} - \gamma \frac{2r_1}{L_1} = 0 \qquad \text{(F-1)}$$

dislocation 2,

$$\Delta\tau b + K \sum_{J>2} \frac{1}{d2j} - K \sum_{J<2} \frac{1}{d2j} = 0 \qquad \text{(F-2)}$$

dislocation 3,

$$\Delta\tau b + K \sum_{J>3} \frac{1}{d3j} - K \sum_{J<3} \frac{1}{d3j} = 0 \qquad \text{(F-3)}$$

dislocation 4,

$$\Delta\tau b + K \sum_{J>4} \frac{1}{d4j} - K \sum_{J<4} \frac{1}{d4j} = 0 \qquad \text{(F-4)}$$

dislocation 5,

$$\Delta\tau b = - K \sum_{J<5} \frac{1}{d5j} + \gamma \frac{2r_5}{L_5} = 0 \qquad \text{(F-5)}$$

where $(\Delta\tau)$ is the order-induced strength increment, $(K) = \frac{Gb^2}{2\pi(1-\nu)}(1 - \nu\cos^2\varphi)$, γ = APB energy, and d_{ij} represents the spacing between dislocations (i) and (j).

Summation of equations (F-1) through (F-5) gives:

$$\Delta\tau = \left(\frac{\gamma}{5b}\right)\left[\frac{2r_1}{L_1} - \frac{2r_5}{L_5}\right]. \qquad \text{(F-6)}$$

(B) Similarly, one may write force balance equations for superdislocations made up of two, three or four dislocations. For a pair of dislocations which are shearing an ordered Ni_4Mo lattice:

Dislocation 1,

$$\Delta\tau b + K \sum_{J>1} \frac{1}{d1J} - \gamma\left(\frac{2r_1}{L_1}\right) = 0 \qquad \text{(F-7)}$$

Dislocation 2,

$$\Delta\tau b - K \sum_{J<2} \frac{1}{d2J} = 0 \qquad \text{(F-8)}$$

Summation of (F-7) and (F-8) yields

$$\Delta\tau = \frac{\gamma}{2b}\left(\frac{2r_1}{L_1}\right) \qquad \text{(F-9)}$$

For three and four dislocations, similar sets of force balance equations yield respectively

$$\Delta\tau = \frac{\gamma}{3b}\left(\frac{2r_1}{L_1}\right) \qquad \text{(F-10)}$$

and

$$\Delta\tau = \frac{\gamma}{4b}\left(\frac{2r_1}{L_1}\right) . \qquad \text{(F-11)}$$

Appropriate methods for calculating $(\Delta\tau)$ from equations (F-6), (F-9), (F-10), and (F-11) are discussed in Chapter II and Appendix D.

BIBLIOGRAPHY

1. V. A. Phillips, Phil. Mag., 16 (1967), 103.

2. L. E. Tanner, Acta. Met., 20 (1972), 1197.

3. H. Gleiter and E. Hornbogen, Mater. Sci. Eng., 2 (1968), 285.

4. R. K. Ham, Proc. 3rd Bolton Landing Conf. (Kear, B. H., et al., eds.) Claitors Publishing Div., Baton Rouge, La., 1970, p. 365.

5. E. Ruedl, P. Delavignette, and S. Amelinckx, Phys. Stat. Sol., 28 (1968), 305.

6. P. R. Okamoto and G. Thomas, Acta. Met., 19 (1971), 825.

7. P. V. Guthrie and E. E. Stansbury, Report ORNL - 3078, Oak Ridge National Laboratory, Oak Ridge, Tennessee, 1961.

8. J. M. Oblak and B. H. Kear, ref. 4, p. 566.

9. F. H. Ellenger, Trans. Am. Soc. Metals, 30 (1942), 607.

10. B. Chakravarti, E. A. Starke, and B. G. LeFevre, J. Mater. Sci., 5, (1970), 394.

11. Fu-Wen Ling and E. A. Starke, Acta. Met., 19 (1971), 759.

12. B. G. LeFevre, H. Grenga, and B. Ralph, Phil. Mag., 18 (1968), 1127.

13. T. Saburi, K. Komatsu, and S. Nenno, Phil. Mag., 20 (1969), 1091.

14. C. R. Brooks and J. E. Spruiell, Mat. Res. Bull., 3 (1968), 381.

15. Strengthening Methods in Crystals, ed. by A. Kelly and R. B. Nicholson, Elsevier Publishing Co., London, 1971.

16. H. Gleiter and E. Hornbogen, Z. Metallk., 58 (1967), 157.

17. J. L. Castagne, J. de Physique, 27 (1966), c. 3.

18. J. M. Oblak, D. F. Paulonis, and D. S. Duvall, Met. Trans., 5 (1974), 143.

19. V. Gerald and H. Haberkorn, Phys. Stat. Sol., 16 (1966), 675.

20. S. M. Copley and B. H. Kear, Trans. Met. Soc. AIME, 239 (1967), 984.

21. E. Hornbogen and M. Roth, Z. Metallkde, 58 (1967), 842.

22. D. Harker, J. Chem. Phys., 12 (1944), 315.

23. A. Kelly and R. B. Nicholson, Precipitation Hardening, Progress in Material Science, The Macmillan Co., vol. 10(3), 1963.

24. P. B. Hirsch and F. J. Humphries, The Physics of Strength and Plasticity, ed. by A. S. Argon, MIT Press, 1969, p. 189.

25. W. B. Snyder and C. R. Brooks, ref. no. 4, p. 365.

26. C. K. H. Dubose and J. O. Steigler, Semi-automatic Preparation of Specimens for T.E.M., ORNL 4066 (February 1967).

27. E. E. Underwood, Quantitative Stereology, Addison-Wesley Publishing Co., 1970.

28. J. E. Spruiell and E. E. Stansbury, J. Phys. Chem. Solids, 26 (1965), 811.

29. P. B. Hirsch, A. Howie, R. B. Nicholson, D. W. Pashley, and M. J. Whelan, Electron Microscopy of Thin Crystals, Butterworths, London, 1965, p. 321.

30. D. F. Paulonis, J. M. Oblak, and D. S. Duvall, Trans. ASM, 62 (1969), 611.

31. L. R. Cornwell, J. D. Embury, and G. R. Purdy, Acta. Met., 18 (1970), 1217.

32. M. Tamura, T. Mori, and T. Nakamura, Trans. Japan Inst. Metals, 14 (5) (1973), 355.

33. I. J. Polmear, J. Aust. Inst. Metals, 11 (4) (1966), 246.

34. B. T. Lampe, M. S. Thesis, Univ. of Tennessee, Knoxville, Tenn. (1963).

35. W. F. Hosford and W. A. Backofen, Proc. of the 9th Sagamore Army Materials Research Conference (W. A. Backofen et al., Eds.), Syracuse University Press (1964), Chapter X.

36. M. H. Lewis and J. W. Martin, Acta Met., 11 (1963), 1207.

37. J. P. Hirth and J. Lothe, Theory of Dislocations, McGraw-Hill Book Company (1968), p. 762.

38. F. R. N. Nabarro, Proc. Roy. Soc. (London), 175A (1940), 519.

39. H. Hu, R. S. Cline, and S. R. Goodman, in Recrystallization, Grain Growth and Textures, Ed. H. Margotin, Amer. Soc. Metals, Metals Park, Ohio (1966), 295.

40. J. E. Spruiell, private communication.

41. E. Orowan, Symposium on Internal Stress in Metals and Alloys, p. 451, 1948, London (Institute of Metals).

42. A. J. E. Foreman and M. J. Makin, Phil. Mag., 14 (1966), 911.

43. H. Gleiter, Acta Met., 16 (1968), 829.

44. P. M. Kelly, International Metallurgical Reviews, 18 (1973), 31.

45. R. K. Ham, Trans. Japan. Inst. Metals, 9 (1968), Suppl., 52.

VITA

John W. Goodrum was born in Athens, Georgia on December 27, 1942. He graduated from Oconee County High School in 1961. He received a B.S. in Chemistry from the University of Georgia in 1965. He attended the University of Georgia from 1965 to 1967 and received an M.S. in Chemistry from that University in 1969. From 1967 to 1971 he served as an officer in the U.S. Air Force, conducting research at the Air Force Cambridge Research Laboratory in Bedford, Massachusetts. In 1971 he was married to the former Rosemarie Farina of Somerville, Massachusetts. From 1971 to 1974, he was engaged in a program of doctoral graduate study at Georgia Institute of Technology.